

UNCLASSIFIED

SECURITY CLASSIFICATION OF THIS PAGE (When Data Entered)

REPORT DOCUMENTATION PAGE		READ INSTRUCTIONS BEFORE COMPLETING FORM
1. REPORT NUMBER Contractor Report CR 79-04	2. GOVT ACCESSION NO.	3. RECIPIENT'S CATALOG NUMBER
4. TITLE (and Subtitle) Dynamical Analysis of Mediterranean Cyclogenesis		5. TYPE OF REPORT & PERIOD COVERED Final
7. AUTHOR(s) Yoshi K. Sasaki (principal investigator) John McGinley		6. PERFORMING ORG. REPORT NUMBER N00228-77-C-3055
9. PERFORMING ORGANIZATION NAME AND ADDRESS University of Oklahoma 200 Felgar Street Norman, OK 73069		10. PROGRAM ELEMENT, PROJECT, TASK AREA & WORK UNIT NUMBERS PE 62759N, PN 9F52551792 NEPRF WU 6.2-5
11. CONTROLLING OFFICE NAME AND ADDRESS Commander, Naval Air Systems Command Department of the Navy Washington, DC 20361		12. REPORT DATE September 1979
14. MONITORING AGENCY NAME & ADDRESS (if different from Controlling Office) Naval Environmental Prediction Research Facility, Monterey, CA 93940		13. NUMBER OF PAGES 52
16. DISTRIBUTION STATEMENT (of this Report) Approved for public release; distribution unlimited.		15. SECURITY CLASS. (of this report) UNCLASSIFIED
17. DISTRIBUTION STATEMENT (of the abstract entered in Block 20, if different from Report)		
18. SUPPLEMENTARY NOTES Original manuscript received in March 1979.		
19. KEY WORDS (Continue on reverse side if necessary and identify by block number) Budget analysis Variational analysis Mediterranean storms Cyclogenesis		
20. ABSTRACT (Continue on reverse side if necessary and identify by block number) Variational calculus methods were developed to study storm development in regions of high terrain. Budget calculations of kinetic energy, latent heat energy and vorticity were made for two cases of a cold front passing over the Alps and into the Mediterranean Sea. The analysis scheme accurately depicted the synoptically significant features while producing relatively small residuals in the budget computations. The results show		

UNCLASSIFIED

SECURITY CLASSIFICATION OF THIS PAGE(When Data Entered)

20. Abstract (Continued)

that kinetic energy in the lower layers was correlated with terrain roughness, where kinetic energy seemed to be damped by mountains. Adiabatic heating in the region of the lee slopes acted to weaken the front while adiabatic cooling in the region of the windward slopes acted to strengthen the front. The increase in moisture condensation in the upslope region acted to slow and intensify the frontal system. These analyses were used to develop a schematic model of the effect of high terrain on frontal movement and intensity.

UNCLASSIFIED

SECURITY CLASSIFICATION OF THIS PAGE(When Data Entered)

AN (1) AD-A076 256
FG (2) 040100
FG (2) 040200
CI (3) (U)
CA (5) OKLAHOMA UNIV NORMAN
TI (6) Dynamical Analysis of Mediterranean Cyclogenesis.
TC (8) (U)
DN (9) Final rept.,
AU (10) Sasaki , Yoshi K.
AU (10) McGinley, John
RD (11) Sep 1979
PG (12) 54p
CT (15) N00228-77-C-3055
PJ (16) F52551
TN (17) WF52551792
RN (18) NEPRF-CR-79-04
RC (20) Unclassified report
DE (23) *Atmospheric physics, *Meteorological data, Storms,
Weather forecasting, Mediterranean Sea, Atmospheric
disturbances, Wind, Atmospheric temperature, Terrain,
Variational methods
DC (24) (U)
ID (25) *Cyclogenesis, PE62759N, WU625
IC (26) (U)
AB (27) Variational calculus methods were developed to study
storm development in regions of high terrain. Budget
calculations of kinetic energy, latent heat energy and
vorticity were made for two cases of a cold front
passing over the Alps and into the Mediterranean Sea.
The analysis scheme accurately depicted the
synoptically significant features while producing
relatively small residuals in the budget computations.
The results show that kinetic energy in the lower
layers was correlated wih terrain roughness, where
kinetic energy seemed to be damped by mountains.
Adiabatic heating in the region of the lee slopes acted
to weaken the front while adiabatic cooling in the



NAVENVPREDRSCHFAC
CONTRACTOR REPORT
CR 79-04
ae
LIBRARY
RESEARCH REPORTS DIVISION
NAVAL POSTGRADUATE SCHOOL
MONTEREY, CALIFORNIA 93940

NAVENVPREDRSCHFAC CR 79-04

DYNAMICAL ANALYSIS OF MEDITERRANEAN CYCLOGENESIS

Prepared By:

Yoshi K. Sasaki and John McGinley

University of Oklahoma
Norman, Oklahoma 73069

Contract No. N00228-77-C-3055

SEPTEMBER 1979

APPROVED FOR PUBLIC RELEASE
DISTRIBUTION UNLIMITED



Prepared For:

**NAVAL ENVIRONMENTAL PREDICTION RESEARCH FACILITY
MONTEREY, CALIFORNIA 93940**

dl

Qualified requestors may obtain additional copies from the Defense Documentation Center. All others should apply to the National Technical Information Service.

CONTENTS

1. INTRODUCTION	1
2. BASIC ANALYSIS	4
3. BUDGET CALCULATIONS	5
3.1 Volume Averages	5
3.2 Energy and Vorticity Equations	6
4. CASE STUDIES	9
REFERENCES	44
APPENDIX A - Use of Variational Inequality Constraints in Adjustment of Vertical Temperature Profiles . . .	45

1. INTRODUCTION

Classical energy and dynamical budgeting studies have traditionally encompassed global or near global regions. Many more recent studies, however, have shown that limited area budgets can provide some excellent insight into phenomena of limited geographical size if:

- a) the boundaries of the system can be defined, and
- b) the horizontal flux through the boundaries can be determined.

While the tropics have provided the greatest potential for limited area budgeting, in this and past work (McGinley, 1973), we consider systems in the westerlies where the boundary flux problem can be significant. This problem is diminished somewhat by the use of high resolution variational analysis schemes.

This present work is a continuation and offshoot of developmental work on a three dimensional analysis procedure for mountainous terrain, including analysis of basic meteorological parameters and computation of terrain induced and mass constrained vertical velocity (Sasaki, et al., 1977). The fine tuning of this scheme continued into the present contract period.

Modifications and improvements to the basic analysis included:

- a) Addition of a strong inequality constraint (see Appendix) to adjust super adiabatic layers arising from the analysis (a manuscript is being prepared for publication).
- b) A routine to extract vertical cross sections from the sigma system. This facilitated case study analysis.

Modifications not completed but under way are:

- a) Merging a first guess field into the analysis scheme for operational use or for extended case studies.
- b) A scheme to remove obviously bad radiosonde data prior to objective analysis.

The budget analysis considered bulk or volume evaluations of fundamental energy and dynamical quantities, including the various forms of energy, vorticity, potential vorticity and frontal intensity. Work by Ninomiya and Matsumoto (1968, 1969) was used as a basis for this work.

In addition, energy and dynamical tendencies evaluated from equations for kinetic, internal, latent heat, vorticity were computed and compared with the bulk energetics and dynamics.

The case studies include:

- a) 6 November 1973, strong cold front crossing Alps into Mediterranean Sea.
- b) 21/22 July 1976, strong summer cold front, over Alps into Mediterranean.

This and succeeding work should serve as a benchmark for numerical studies conducted by others (Buzzi and Tribaldi, 1977; Trevisan, 1976; and Bleck, 1977). The problem of Mediterranean cyclogenesis is a complex one involving a mountain range of sub-synoptic scale, a persistent thermal and latent heat energy gradient and abundant upper level disturbances moving into the area from the northwest to west. The energetic and dynamic influences of these stationary terrain features figure prominently in the consequent development and modification of moving weather systems. Hopefully some measure of these effects and speculations regarding their origin can be made within this report.

2. BASIC ANALYSIS

[For details, see (Sasaki, et al., 1977)]

The analysis scheme uses twice a day radiosonde observations subjecting the data to the following:

- a) Variational low pass filtering to smooth the data.
- b) Adjustment of vertical temperature profiles using inequality constraint (see Appendix).
- c) Geostrophic and hydrostatic adjustment of the geopotential field.
- d) Calculation of surface pressure at the ground surface.
- e) Coordination of transformation from π ($= \ln P_0/P$) to σ (sigma) in the vertical.
- f) Application of mass constraint on the wind field in the $[x, y, \sigma]$ domain.
- g) Computation of ω (omega) vertical motion fields.
- h) Computation of vorticity and potential vorticity.
- i) Vertical cross-sections.

3. BUDGET CALCULATIONS

3.1 VOLUME AVERAGES

Quantities are averaged over volume elements within the main three dimensional analyzed domain. Each meteorological variable (A) is averaged in the horizontal and vertical according to:

$$\bar{A}_i^{xy} = \frac{1}{s} \int_s A \, dx \, dy$$

(where s is the horizontal area of the volume at level i)

and

$$\bar{A}^{\text{vol}} = \frac{1}{1-\sigma_T} \int_1^{\sigma_T} \left[\frac{\bar{A}_i^{xy} + \bar{A}_{i+1}^{xy}}{2} \right] d\sigma$$

(where \bar{A} is the volume average and σ_T is the topmost σ level).

Note that the averages in the sigma system are implicitly mass weighted since each layer of fixed depth $\Delta\sigma$ has the same mass/per unit area, when we consider some mean surface pressure for the volume.

Averages are computed with n volumes and sub-elements for quantities of particular meteorological interest, such as temperature (enthalpy), geo-potential (potential energy), wind (kinetic energy), moisture-mixing ratio (latent heat), vorticity, potential vorticity and frontal intensity (defined as $\frac{\partial \theta}{\partial n}$, where n is the horizontal normal to the frontal surface).

3.2 ENERGY AND VORTICITY EQUATIONS

Equations for the energy calculations were taken from Haltiner (1971) and McGinley (1973) and modified to include Flux, Eulerian and Lagrangian forms in the σ system.

1. For Kinetic Energy

- a) Flux form (can be integrated to compute vertical flux and can evaluate eddy or subgrid fluxes).

$$\frac{\partial K}{\partial t} + \nabla_{\sigma} \cdot (K \vec{V} + P_s \Phi \vec{V}) + \frac{\partial}{\partial \sigma} (K \dot{\sigma} + P_s \Phi \dot{\sigma}) + \frac{\partial P_s}{\partial t} \frac{\partial \Phi}{\partial \sigma} - \frac{\partial \Phi}{\partial \sigma} = 0$$

(where K is kinetic energy per unit mass, P_s is surface pressure, Φ is geopotential of constant σ surface, \vec{V} is velocity, ω is $\frac{dP}{dt}_{\sigma}$, $\dot{\sigma}$ is $\frac{d\sigma}{dt}$. The relation between ω (omega) and $\dot{\sigma}$ is $(\omega)_{\sigma} = P_s \dot{\sigma} + P_s \dot{\sigma} \sigma$. In addition, we compute the local tendency of kinetic energy, $\frac{\partial K}{\partial t}$; the Lagrangian form $\frac{dK}{dt}$; and the parcel of budget volume form, $\frac{DK}{Dt}$, where the change is defined with respect to an arbitrary moving element.

2. For Thermal Energy

- a) The Flux form:

$$\frac{\partial}{\partial t} (C_p P_s T) + \nabla \cdot (C_p P_s T \vec{V}) + \frac{\partial}{\partial \sigma} (C_p P_s T \dot{\sigma}) - \pi \omega \omega = \frac{SP}{\rho}$$

where T is temperature, S is a non adiabatic heat source, C_p is the specific heat at constant pressure, and ρ is density. We also compute:

$$\frac{\partial (C_p P_s T)}{\partial t}, \frac{d(C_p P_s T)}{dt}, \frac{D(C_p P_s T)}{DT}$$

3. For Latent Heat Energy

a) Flux form:

$$\frac{\partial (LqP_s)}{\partial t} + \nabla \cdot (LP_s q \vec{V}) + \frac{\partial}{\partial \sigma} (LP_s q \dot{\sigma}) = -\frac{P_s LS}{\rho}$$

(where q is mixing ratio and LS is a latent heat sink term).

Again, as in 1. and 2. we compute

$$\frac{\partial L}{\partial t}, \frac{d L}{dt}, \frac{D L}{Dt}$$

4. Vertical Fluxes

We can integrate Equation 1 to find $(P_s K \dot{\sigma})_\sigma$, the vertical kinetic energy flux. By combining Equations 2 and 3 and assuming that S represents moisture processes only, we find the vertical heat flux:

$$\dot{\sigma} P_s (L_q + C_p T)_\sigma$$

5. Vorticity Equations

Vorticity (a) and potential vorticity (b) are computed as:

$$a) \zeta = \frac{\partial v}{\partial y} - \frac{\partial u}{\partial x} + \frac{u \tan \phi}{Re} + \left[\frac{\partial v}{\partial \sigma} \frac{\partial \sigma}{\partial y} \right]_p - \left[\frac{\partial u}{\partial \sigma} \frac{\partial \sigma}{\partial x} \right]_p$$

where Re is earth radius, ϕ is latitude, and the bracketed term is the correction due to the σ system.

$$b) P = \zeta \frac{\partial \theta}{\partial p} = \frac{\zeta}{P_s} \frac{\partial \theta}{\partial \sigma}, \quad \theta \text{ is potential temperature.}$$

The vorticity equation in the pressure system is transformed into the sigma coordinate system, so that we may evaluate vorticity tendency and quantify the role of each term in vorticity production.

$$\begin{aligned}
 \frac{\partial \zeta}{\partial t} + \vec{v} \cdot \nabla_{\sigma} (\zeta + f) - \frac{\sigma \partial (\zeta + f)}{p_s} \vec{v} \cdot \nabla p_s + \frac{\omega}{p_s} \frac{\partial \zeta}{\partial \sigma} & \text{ Advection term.} \\
 + (f + \zeta) \nabla_{\sigma} \cdot \vec{v} - \frac{\sigma}{p_s} \nabla p_s \cdot \frac{\partial \vec{v}}{\partial \sigma} & \text{ Divergence term.} \\
 + \frac{1}{p_s} \left(\frac{\partial \omega}{\partial y} \frac{\partial u}{\partial \sigma} - \frac{\partial \omega}{\partial x} \frac{\partial v}{\partial \sigma} + \frac{\partial u}{\partial \sigma} \frac{\partial \omega}{\partial y} \frac{\partial \sigma}{\partial y} \right)_p - \frac{\partial v}{\partial \sigma} \frac{\partial \omega}{\partial \sigma} \frac{\partial \sigma}{\partial x})_p & \text{ Tilting term.}
 \end{aligned}$$

4. CASE STUDIES

As stated in the Introduction the motivation for this work is to quantify some of the changes associated with air-flow interacting with a mountain barrier, specifically modification to frontal boundaries as they pass over a significant range.

Figure 1 shows the region of analysis and data density along with terrain height.

In each time period we will be evaluating changes averaged within large volumes associated with surface and upper level frontal zones. These volumes are positioned subjectively and are large to insure reasonable bulk evaluations of energy and dynamical quantities. A similar technique was used by McGinley (1973). Figure 2 shows schematically how the volume is placed over a frontal surface moving with the mean frontal velocity over the time period.

The geography of the Mediterranean region is unique and configured in such a way that frontal zones either pass over low hills in moving southeastward from the Atlantic to the Mediterranean, or very sharp mountain ranges (the Alps or Pyrenees) along adjacent trajectories. We shall make use of cross-section analysis to compare the "mountain" versus "low

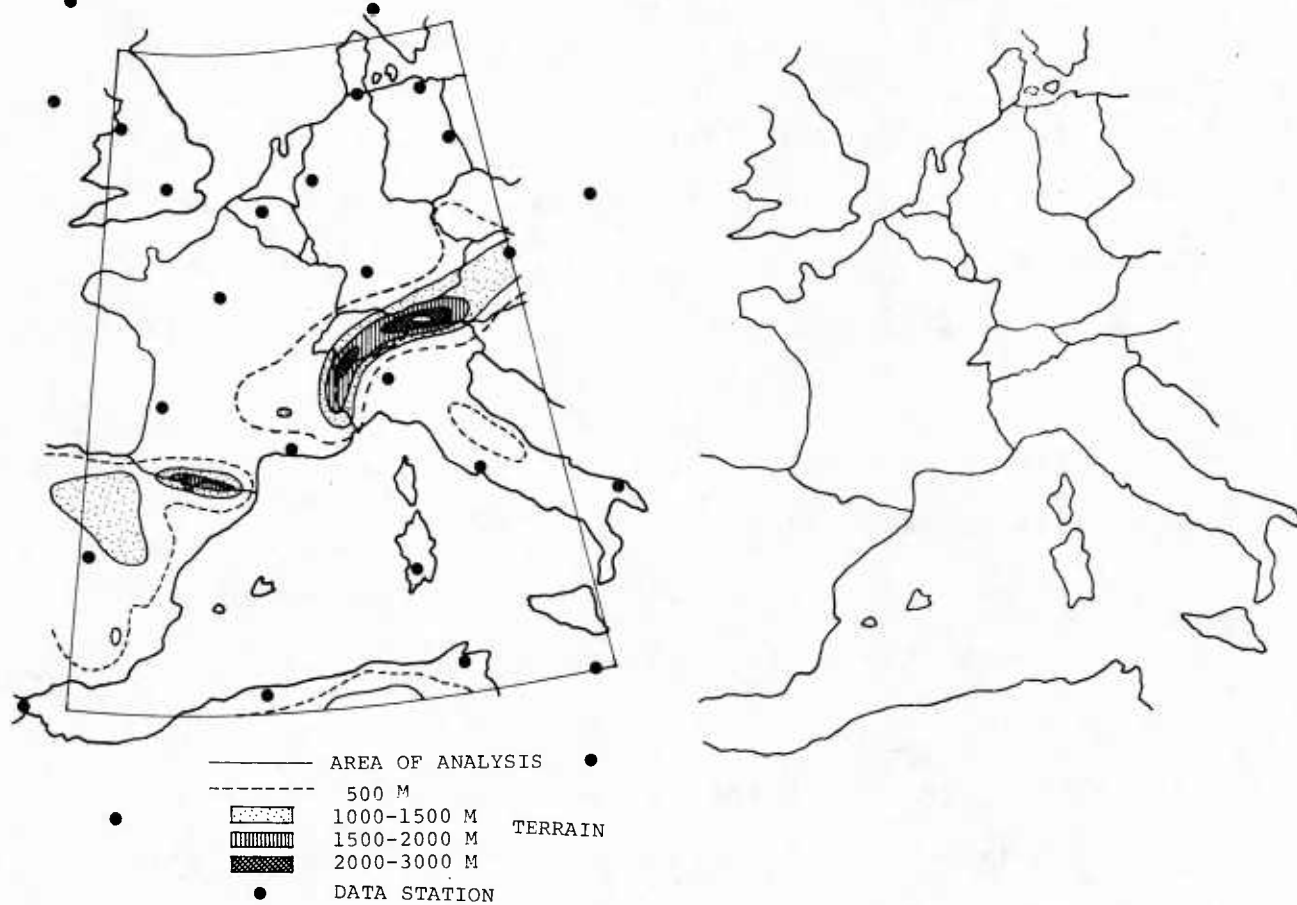


Fig. 1. Region of Analysis, Rawinsonde Stations and Terrain Heights (m). See key.

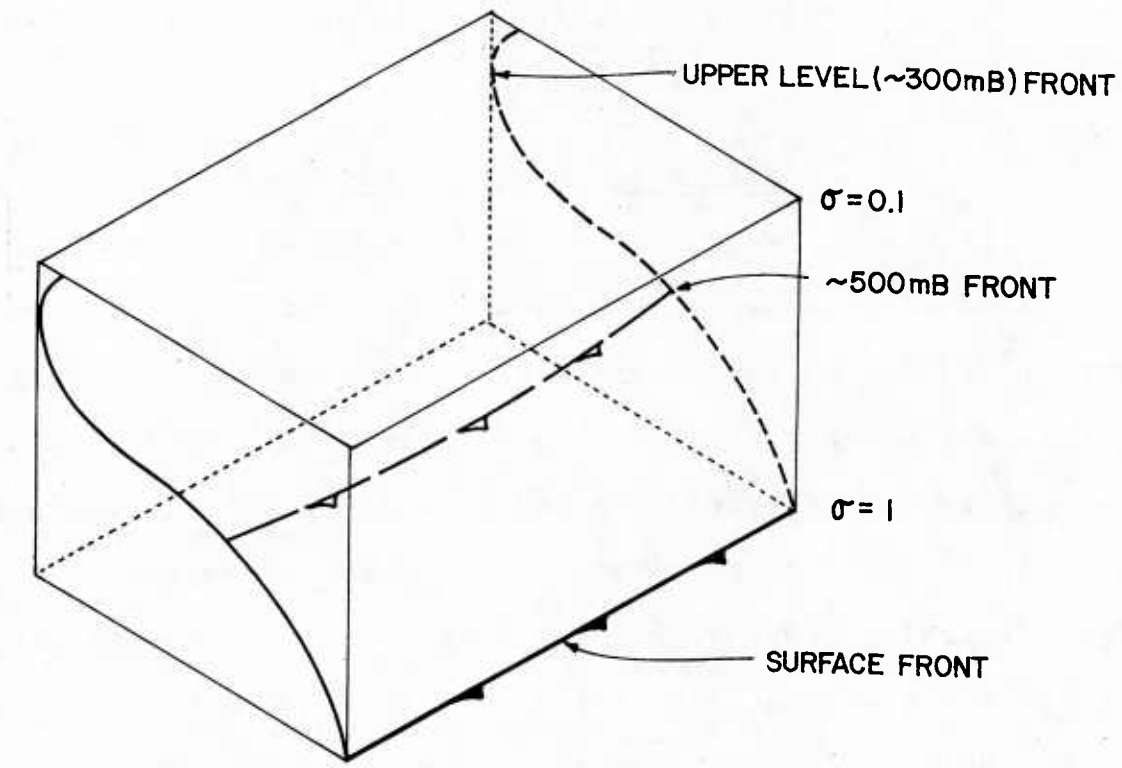


Fig. 2. Placement of budget volume relative to frontal boundary (surface and 500 mb fronts are illustrated). Volume propagates with movement of frontal surface.

"terrain" fronts, in addition to comparing their bulk properties. In both case studies volume A will be associated with the Alps, volume B associated with the Pyrenees, and volume C the terrain of southern France.

Case 1, 6 November 1973

Figures 3 and 4 show frontal positions at surface and middle levels, jetstream positions and vertical motion fields for 00 and 12Z. The frontal surface moves over the mountain ranges during this time period. The frontal zone is divided into three volume elements A and B, which pass over the Alps and the Pyrenees respectively, and C which moves over the lower terrain between. Figures 5, 6 and 7 show changes of energy and dynamical quantities with respect to these volumes.

Note how kinetic energy in the lower half of volumes A and B decrease while kinetic energy in the upper half increases. In volume C we note less kinetic energy change proportionately.

Mean vertical motion increases in A and B while decreasing in C over the 12 hour period. The effect of vertical motion within the volume is to increase available potential energy by increasing the strength of frontal zones. This is seen in volume A, Figure 5 where middle and upper fronts intensify while the front at low levels weakens. In volume C the opposite is observed as the lower front increases with respect to a weakening upper front.

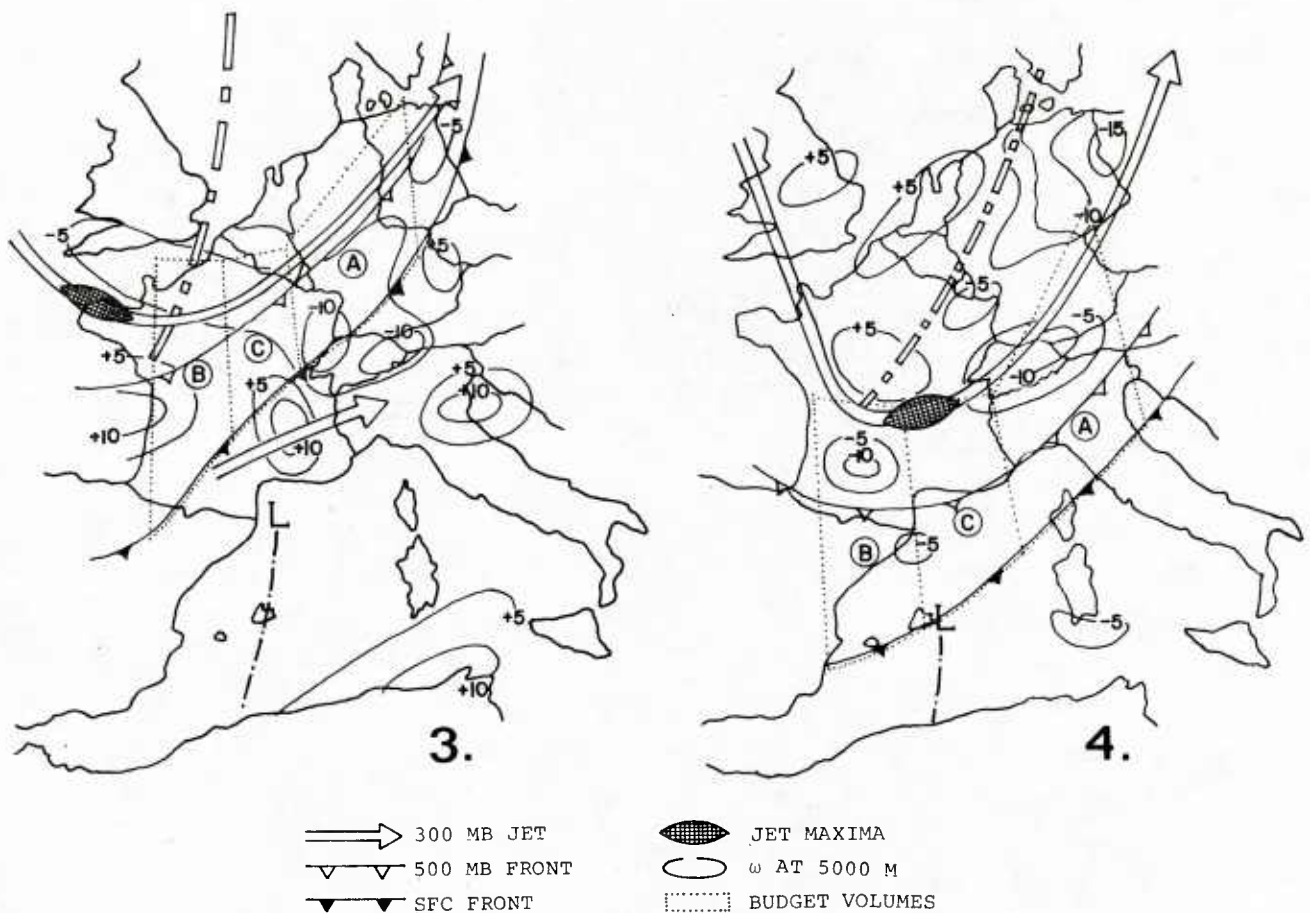
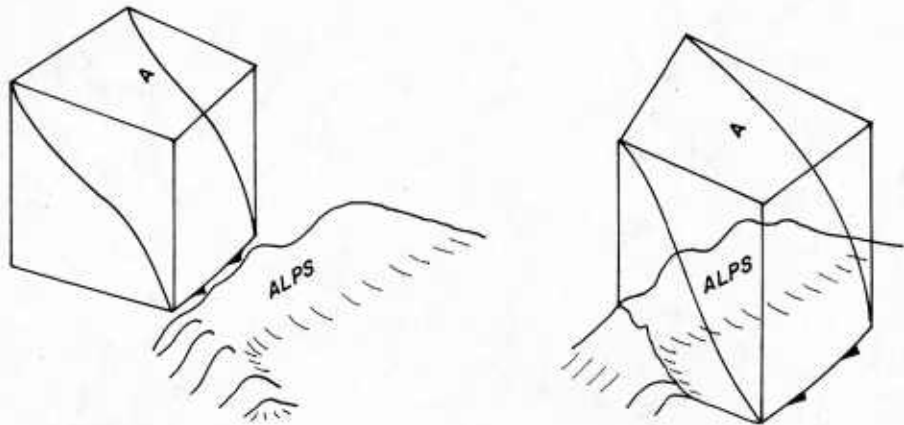


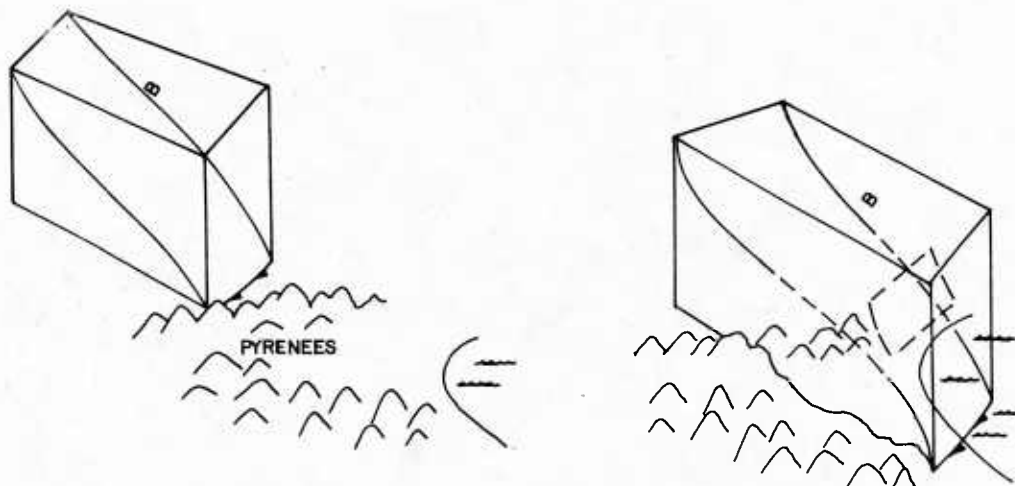
Fig. 3. Composite chart illustrating surface and 500 mb frontal position; budget Volumes A, B, C; Tropospheric jet axis and wind maxima; and vertical motion ($\text{mb}^{-3}/\text{sec}$) for 00Z 6 Nov. 73 (see key).

Fig. 4. Composite chart illustrating surface and 500 mb frontal position; budget volumes A, B, C; Tropospheric jet axis and wind maxima; and vertical motion ($\text{mb}^{-3}/\text{sec}$) for 12Z 6 Nov. 73 (see key).



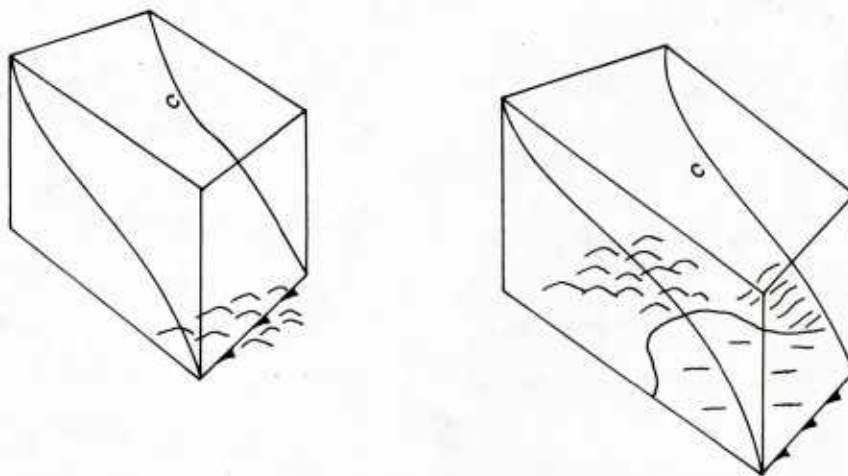
<u>MEAN QUANTITY</u>	<u>00Z</u>	<u>12Z</u>	<u>12 HR. CHANGE</u>
ω (MBAR/SEC $\times 10^{-3}$)	-1.4	-2.7	-1.3
KE (CAL/GRM)	.088	.096	+ .008
UPPER HALF	.123	.160	+ .037
LOWER HALF	.053	.031	- .022
INTERNAL (CAL/GRM)	59.740	58.500	-1.24
POTENTIAL (CAL/GRM)	13.800	15.000	+1.20
LATENT HEAT (CAL/GRM)	1.13	1.19	+ .06
ABS. VORT. ($SEC^{-1} \times 10^{-5}$)	12.5	11.2	-1.3
REL. VORT. ($SEC^{-1} \times 10^{-5}$)	1.2	.5	- .7
UPPER HALF	-1.3	2.3	+3.6
LOWER HALF	3.3	-1.4	-4.7
FRONTAL INTENSITY [$-\frac{\partial \theta}{\partial Y}$] (°C/111KM)	3.1	4.1	+1.0
UPPER HALF	4.0	5.7	+1.7
LOWER HALF	2.2	2.5	+ .3

Fig. 5. Schematic of Volume A (containing frontal zone) passing over Alps. Table lists mass weighted volume averages for 00 and 12Z 6 Nov. 73 and time changes in: vertical motion; kinetic energy (in upper and lower half of volume), other energy quantities; absolute and relative vorticity (in upper and lower half); and frontal intensity (in upper and lower half).



<u>MEAN QUANTITY</u>	<u>00Z</u>	<u>12Z</u>	<u>12 HR. CHANGE</u>
ω (MBAR/SEC $\times 10^{-3}$)	- .6	-1.7	-1.1
KE (CAL/GRM)	.053	.046	- .007
UPPER HALF	.083	.077	- .006
LOWER HALF	.024	.016	- .008
INTERNAL (CAL/GRM)	59.95	60.08	+ .13
POTENTIAL (CAL/GRM)	13.47	14.13	+ .56
LATENT HEAT (CAL/GRM)	1.19	1.02	- .17
ABS. VORT. ($SEC^{-1} \times 10^{-5}$)	13.5	11.8	-1.7
REL. VORT. ($SEC^{-1} \times 10^{-5}$)	2.4	1.9	- .5
UPPER HALF	3.0	3.5	+ .5
LOWER HALF	1.2	0.2	-1.0
FRONTAL INTENSITY [$\frac{\partial \theta}{\partial Y}$] ($^{\circ}\text{C}/111 \text{ KM}$)	3.0	3.0	0
UPPER HALF	4.0	5.8	+1.8
LOWER HALF	1.9	.2	-1.7

Fig. 6. Schematic of Volume B (containing frontal zone passing over Pyrenees. Table lists mass weighted volume averages for 00 and 12Z 6 Nov. 73 and time changes in: vertical motion; kinetic energy (in upper and lower half of volume), other energy quantities; absolute and relative vorticity (in upper and lower half); and frontal intensity (in upper and lower half).



<u>MEAN QUANTITY</u>	<u>00Z</u>	<u>12Z</u>	<u>12 HR. CHANGE</u>
ω (MBAR/SEC $\times 10^{-3}$)	- .6	-1.7	-1.1
KE (CAL/GRM)	.053	.046	- .007
UPPER HALF	.083	.077	- .006
LOWER HALF	.024	.016	- .008
INTERNAL (CAL/GRM)	59.95	60.08	+ .13
POTENTIAL (CAL/GRM)	13.47	14.13	+ .56
LATENT HEAT (CAL/GRM)	1.19	1.02	- .17
ABS. VORT. ($SEC^{-1} \times 10^{-5}$)	13.5	11.8	-1.7
REL. VORT. ($SEC^{-1} \times 10^{-5}$)	2.4	1.9	- .5
UPPER HALF	2.8	6.1	+3.3
LOWER HALF	3.7	2.6	-1.1
FRONTAL INTENSITY $[-\frac{\partial \theta}{\partial Y}]$ ($^{\circ}C/111KM$)	3.1	4.5	+1.4
UPPER HALF	4.0	5.0	+1.0
LOWER HALF	1.9	4.3	+2.4

Fig. 7. Schematic of Volume C moving into Mediterranean. Table lists mass weighted volume averages for 00 and 12Z 6 Nov. 73 and time changes in: vertical motion; kinetic energy (in upper and lower half of volume), other energy quantities; absolute and relative vorticity (in upper and lower half); and frontal intensity (in upper and lower half).

Cross sections through each volume are shown in Figures 8 through 13. Note how, in B (Figures 10 and 11), the upper front strengthens while the lower front appears to decouple and weaken. A similar trend is seen in A (Figures 8 and 9).

The net loss of vorticity and potential vorticity in A and B at low levels appears to be related to the same mechanism (frictional effect), which is reducing the kinetic energy. Evaluation of vorticity tendencies for each data time could not isolate the term responsible for this loss, so frictional dissipation may be the mechanism.

Lagrangian tendencies of KE and heat (Figures 14 and 15) show how the terrain influences the air parcels. Values shown are for columns one meter square and as deep as the analyzed atmosphere. Note how at 00 and 12Z the mountain ranges act as KE sinks. This supports the results of the bulk calculations in Figures 5, 6 and 7. In addition the forcing of air over the mountain cools air on the windward side and warms air on the leeward side. Mountain ranges are frontogenetic in this respect. Figures 10 and 11 illustrate how a weak low level front is enhanced within B, as northerly flow passes over the mountain barrier.

Case 2, 21/22 July 1976

Figures 16 and 17 show the synoptic features on 21 July/12Z and 22 July/00Z. The front interacts with the mountain ranges in a very similar way to Case 1. Volumes A, B and C are assigned to appropriate frontal elements.

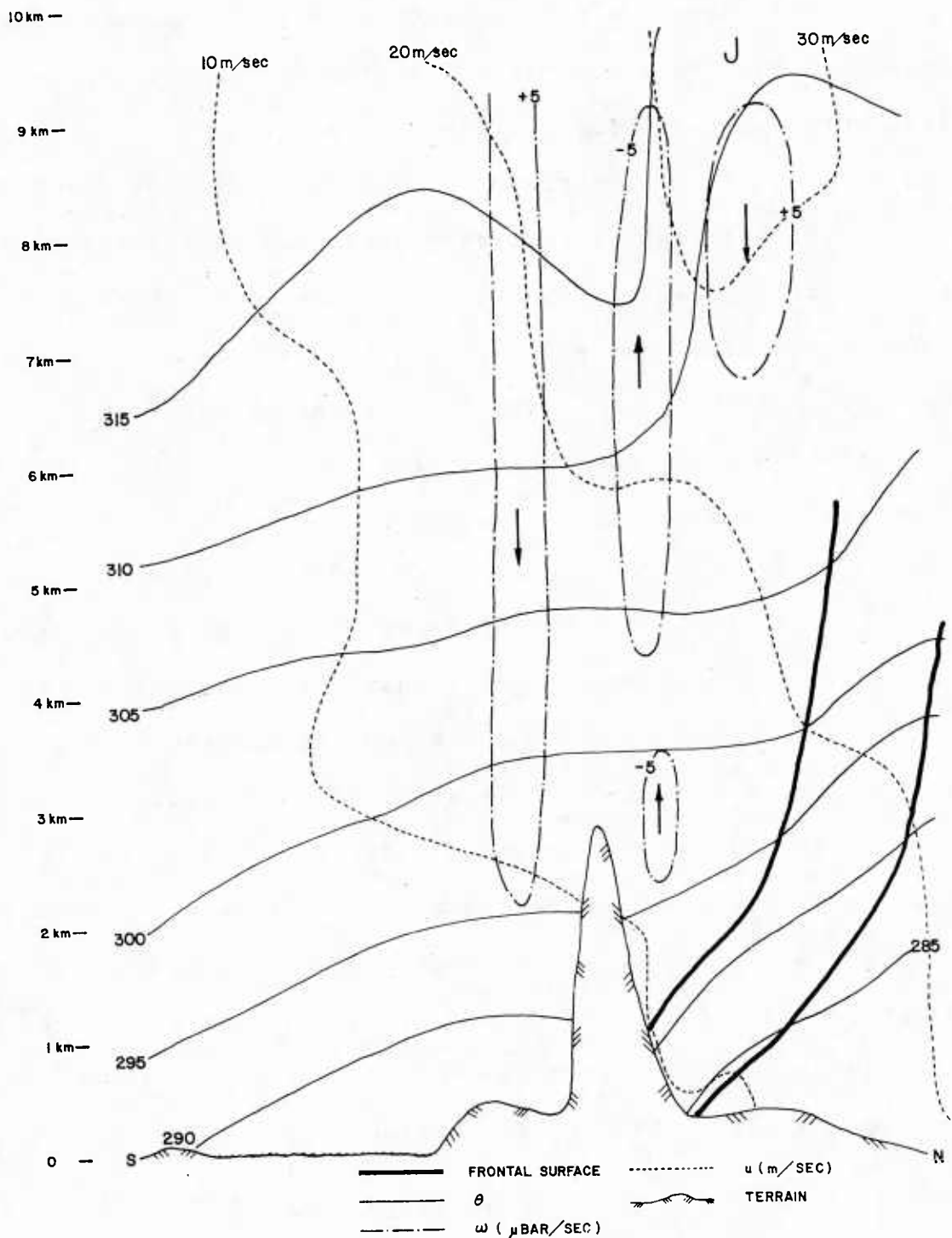


Fig. 8. Cross section through Volume A (along 11E) from 36° N to 55° N, illustrating frontal zone, potential temperature (θ), vertical motion (ω) and westerly wind component (u) for 00Z 6 Nov. 73.

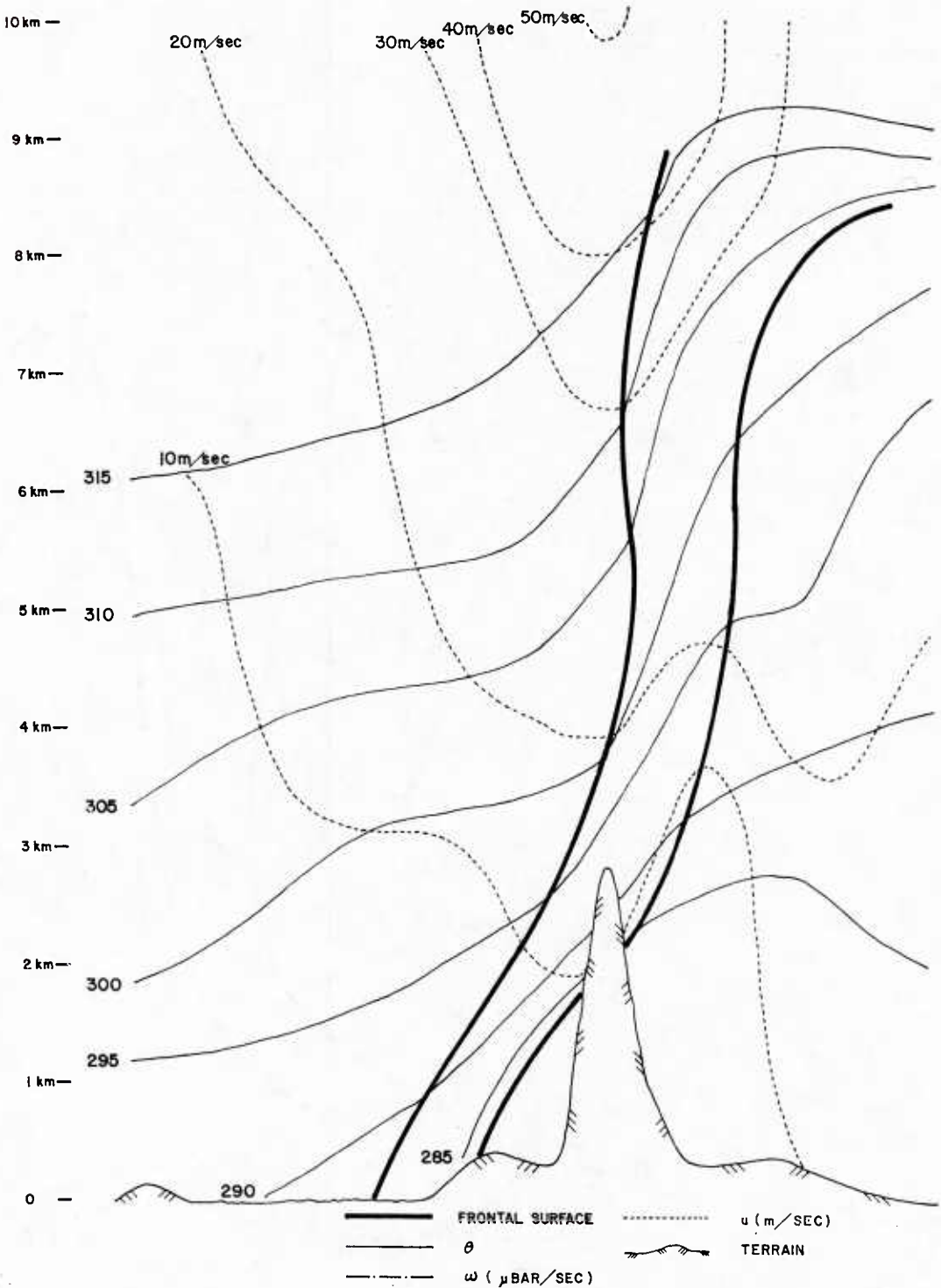


Fig. 9. Cross section through Volume A (along 11 E) from 36° N to 55° N, illustrating frontal zone, potential temperature (θ), vertical motion (ω) and westerly wind component (u) for 12Z 6 Nov. 73.

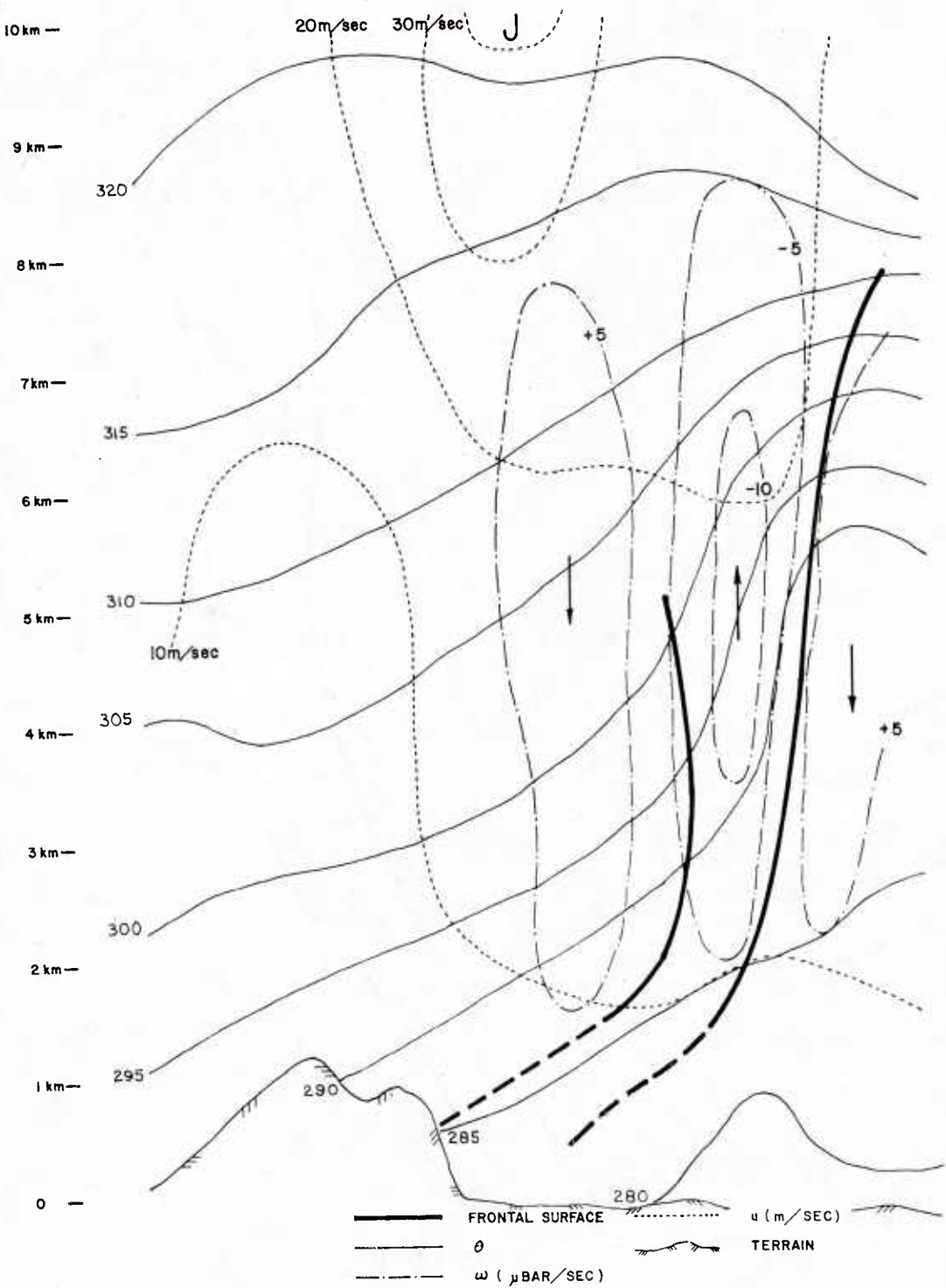


Fig. 10. Cross section through volume B (along 1° W) from 36° N to 55° N illustrating frontal zone, potential temperature (θ), vertical motion (ω) and westerly wind component (u) for 00Z 6 Nov. 73.

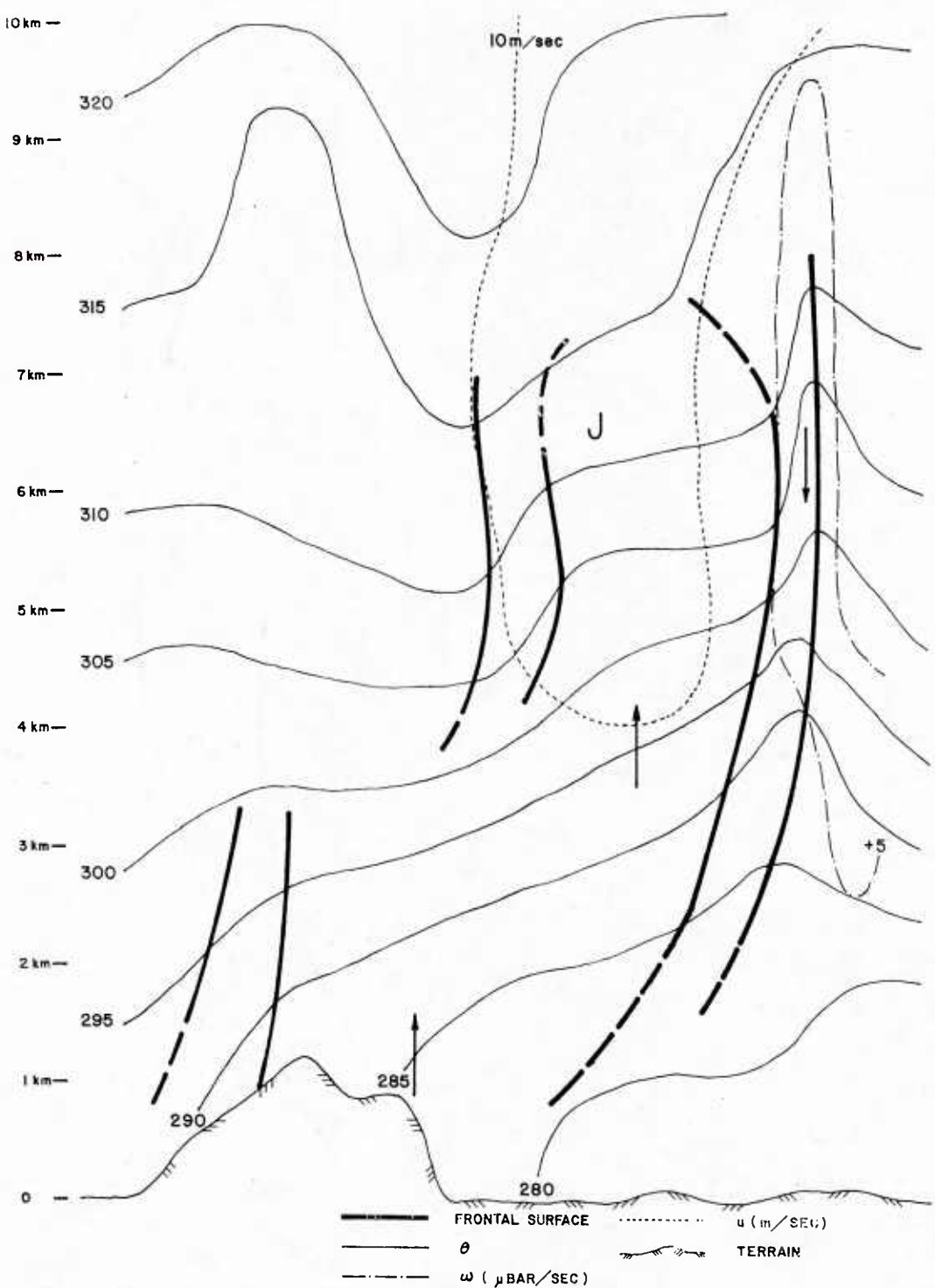


Fig. 11. Cross section through Volume B (along 1° W) from 36° N to 55° N illustrating frontal zone, potential temperature (θ), vertical motion (ω) and westerly wind component (u) for 12Z 6 Nov. 73.

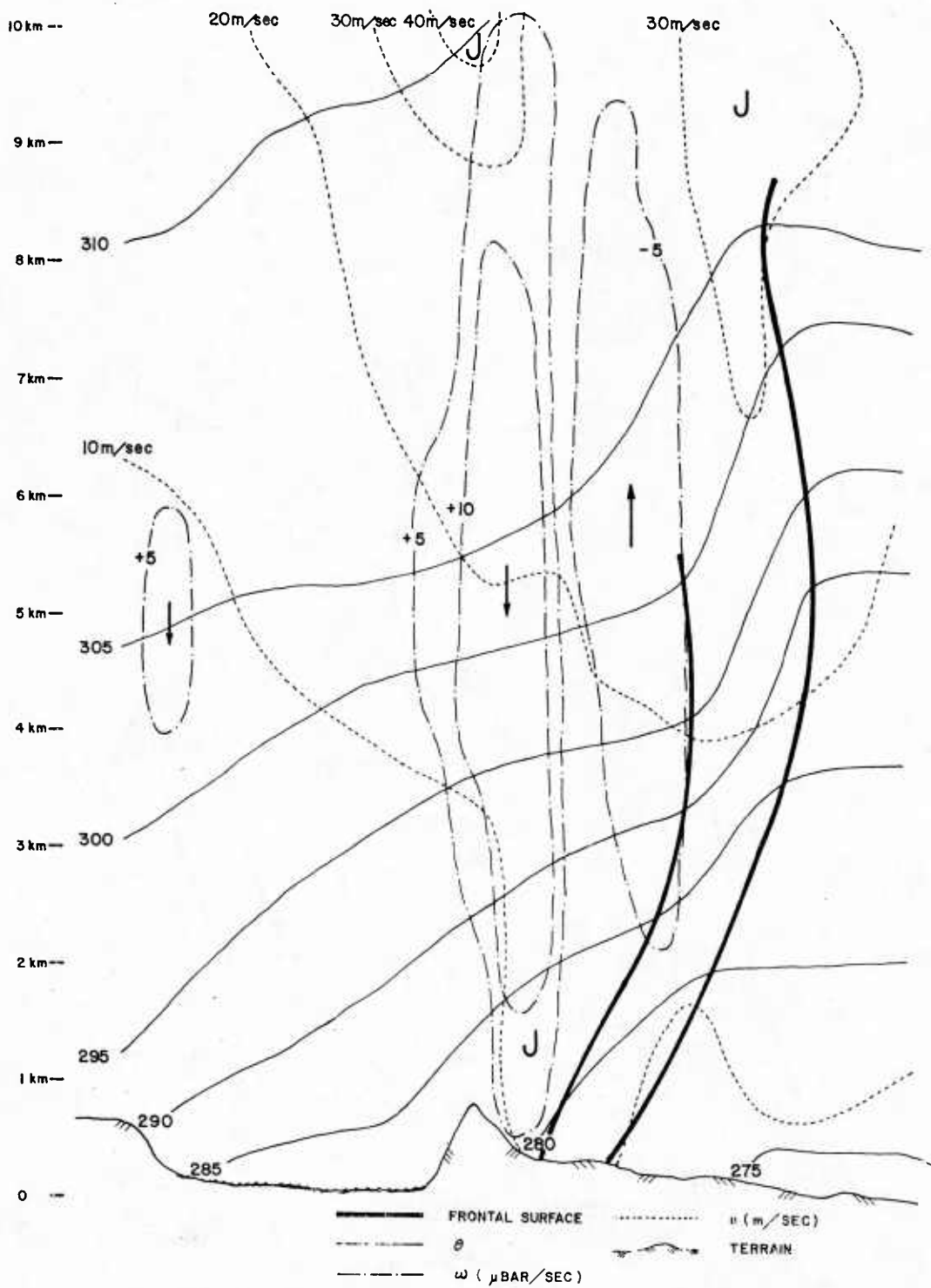


Fig. 12. Cross section through Volume C (along 5° E) from 36° to 55° N illustrating frontal zone, potential temperature (θ), vertical motion (ω) and westerly wind component (u) for 00Z 6 Nov. 73.

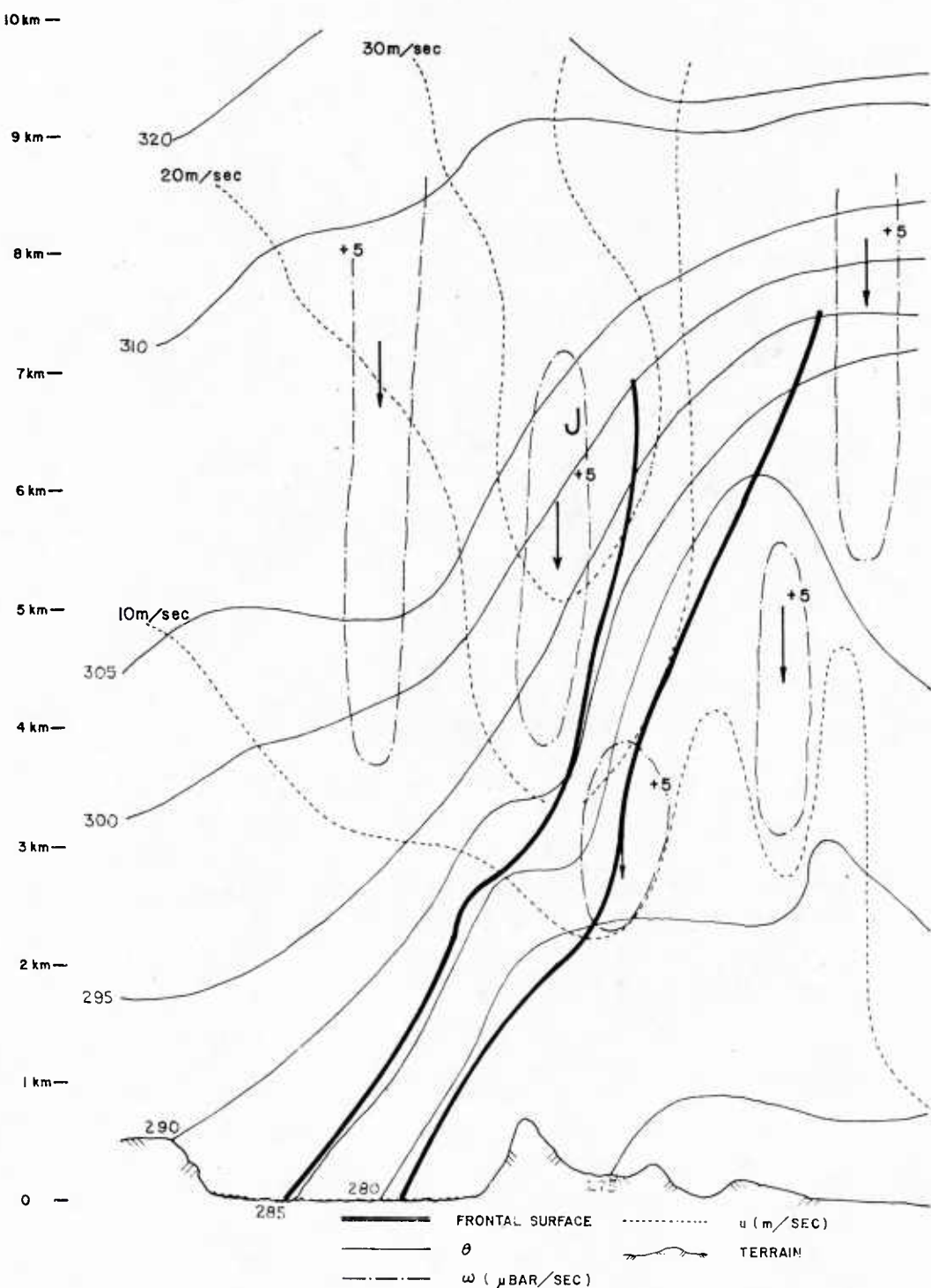


Fig. 13. Cross section through Volume C (along 5° E) from 36° to 55° N illustrating frontal zone, potential temperature (θ), vertical motion (ω) and westerly wind component (u) for 12Z 6 Nov. 73.

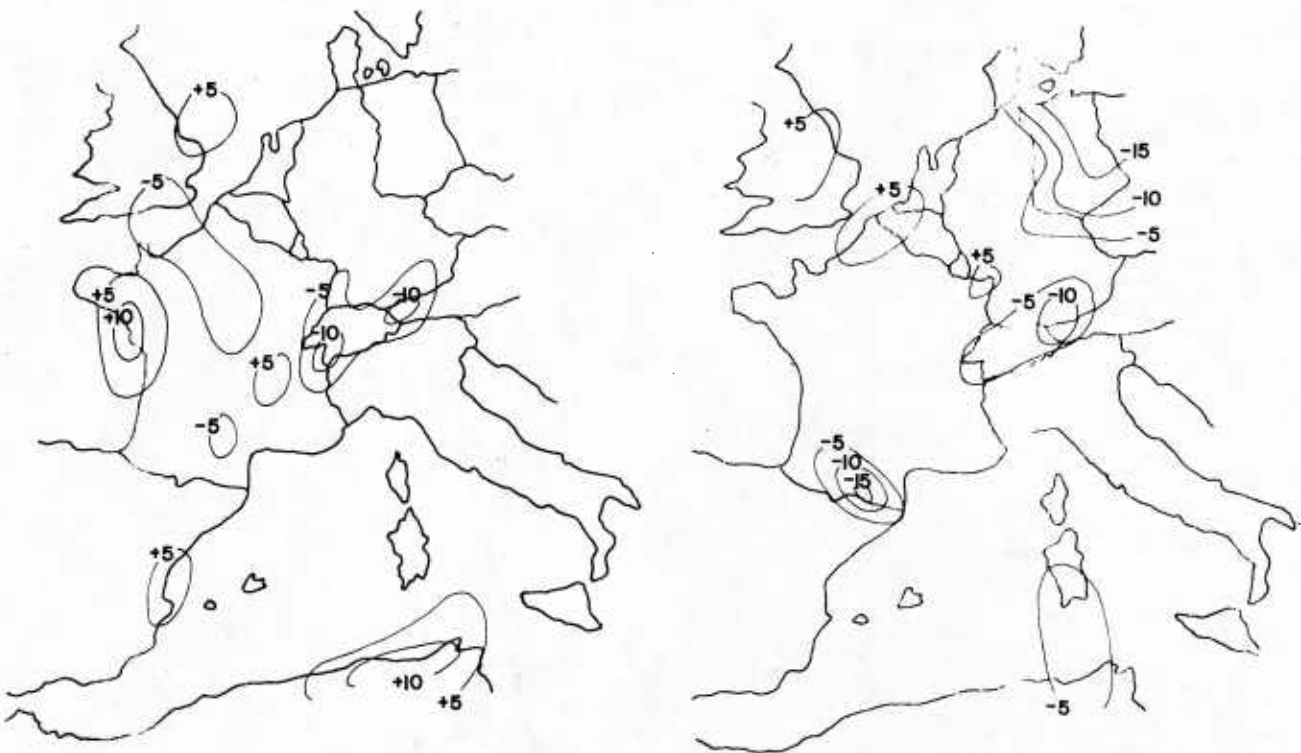


Fig. 14. Lagrangian kinetic energy tendency through whole atmospheric depth. For 6 Nov. 73.

$$\left[\frac{d\left(\frac{1}{2}v^2 P_s \right)}{dt} \right] \text{ (cal/m}^2 \text{ sec} \times 10^4 \text{)}$$

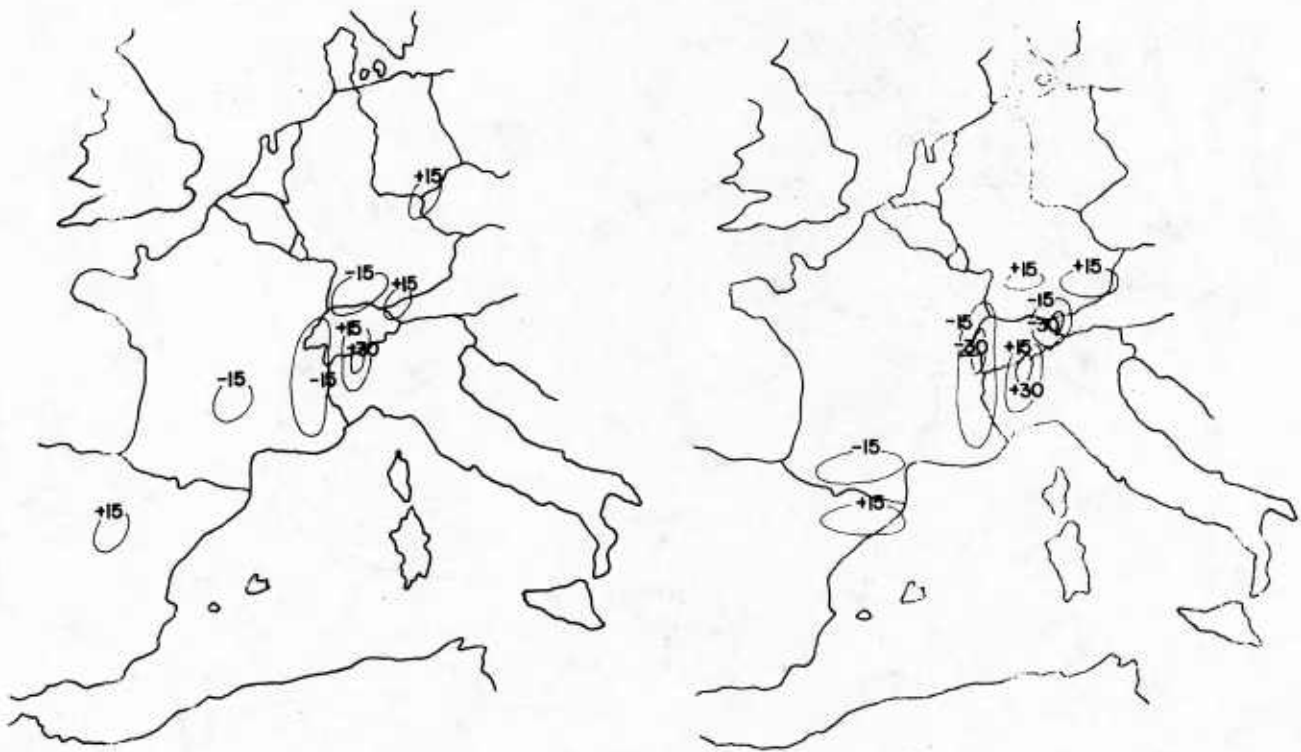
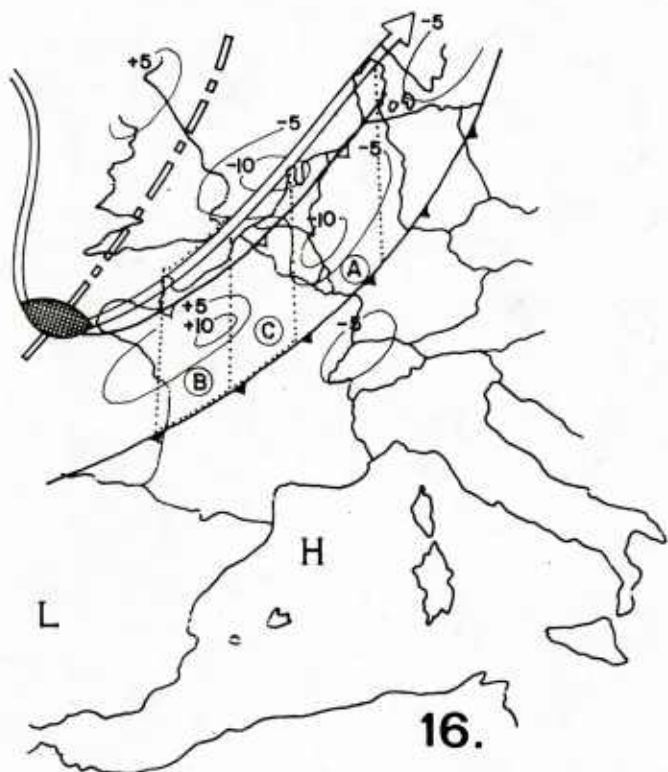


Fig. 15. Lagrangian enthalpy tendency through whole atmospheric depth for 6 Nov. 73.

$$[\frac{d(C_{TP})}{dt}] \text{ (cal/m}^2\text{ sec} \times 10^4)$$



→ 300 MB WIND BAND ▽ 500 MB FRONT
 —— 500 MB TROUGH ▾ SFC FRONT
 (C) ω IN $\text{MB} \times 10^{-3}/\text{SEC}$ ◻ WIND MAXIMA

Fig. 16. Composite chart illustrating surface and 500 mb frontal position; budget Volumes A, B, C; Tropospheric jet axis and wind maxima; and vertical motion ($\text{mb}^{-3}/\text{sec}$) for 12Z 21 July 76.

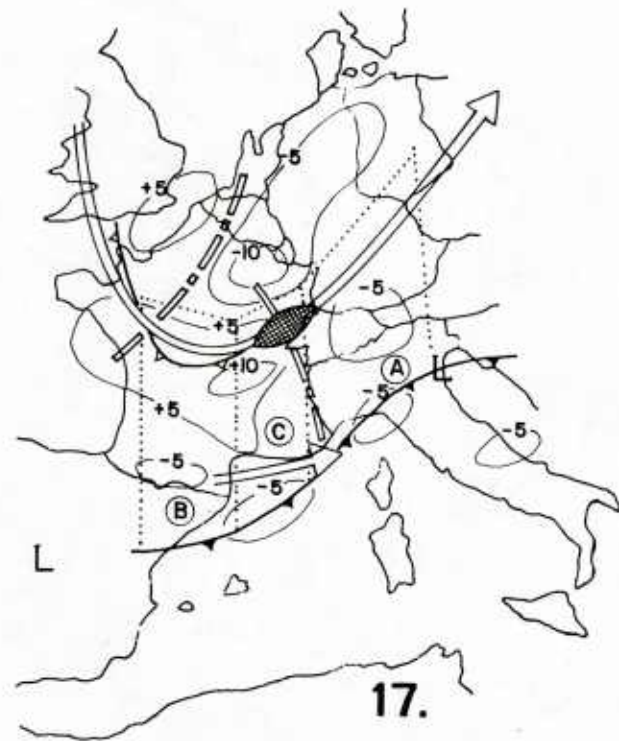


Fig. 17. Composite chart illustrating surface and 500 mb frontal position; budget Volumes A, B, C; Tropospheric jet axis and wind maxima; and vertical motion ($\text{mb}^{-3}/\text{sec}$) for 00Z 22 July 76.

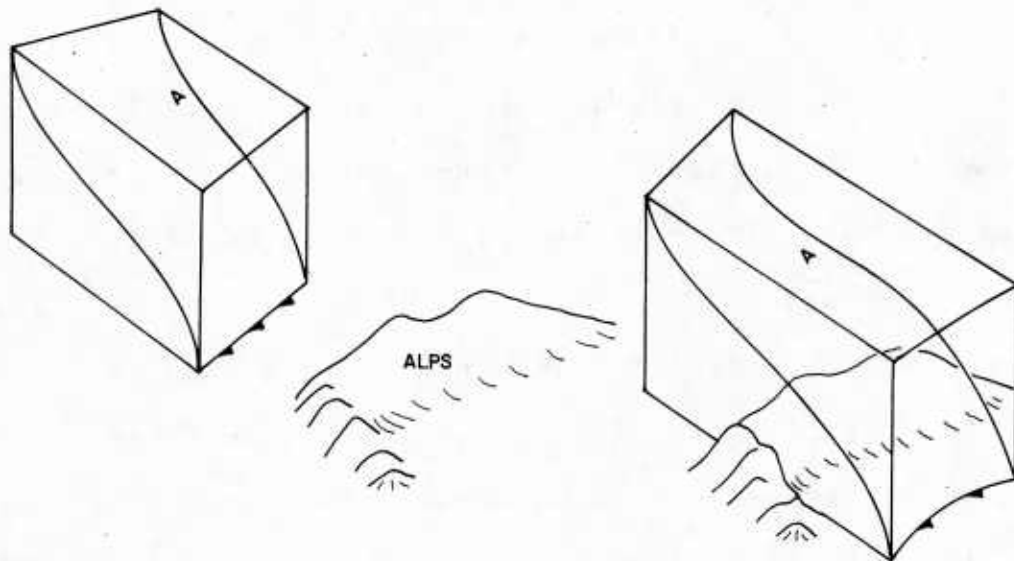
Some similarities are observed (Figures 18 through 26). The lower level kinetic energy and vorticity is diminished most significantly in mountain regions. Frontal intensity increases in that part of the front directly over the mountain crest.

The dynamical forcing induced by a wind speed maxima in the upper flow is clearly seen in Figure 27 as a couplet of increasing/decreasing KE tendencies as air accelerates upstream of the maximum and decelerates downstream. This is consistent with models of wind maxima (Palmein and Newton, 1969). This couplet moves across Europe, contrasting with the non-moving sinks associated with the mountains. Figure 28 shows the influence of the mountains on heating and cooling of parcels.

Conclusion

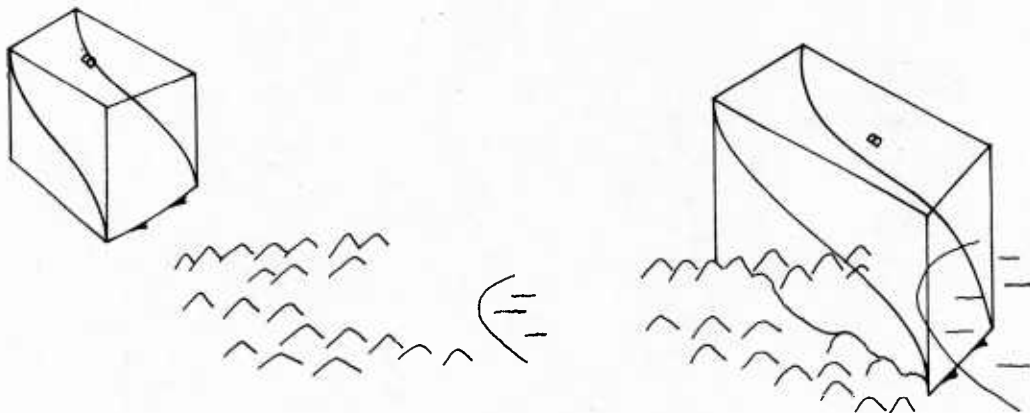
While the study completed is not thorough enough to support broad generalizations, some useful findings did result.

- a) The analysis scheme, in terms of positioning of meteorological features (frontal positions, jet positions, vertical motion fields) seem to be excellent. The w patterns were quite good in comparison with obvious upper level frontogenetic processes and terrain features. The cross section analyses confirm this quite well. This study has increased confidence in the use of basic analysis scheme.



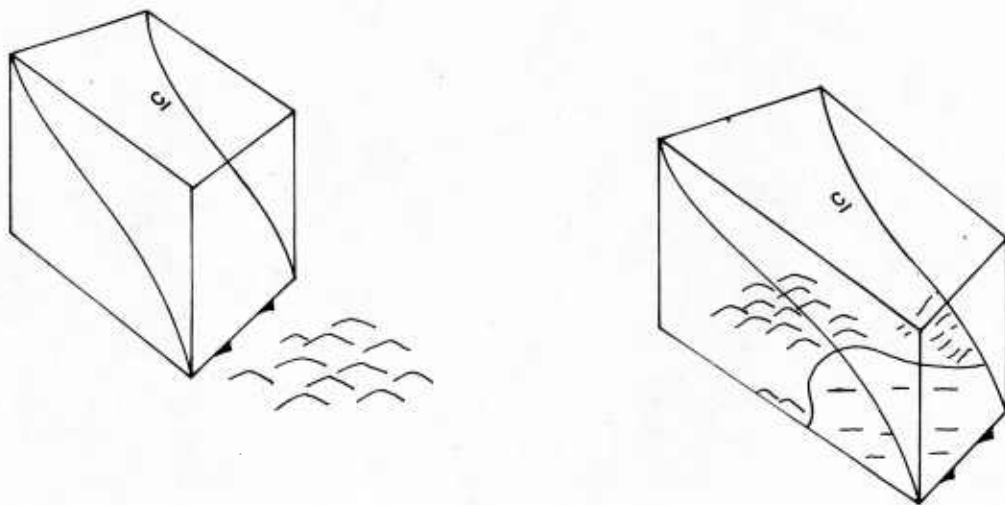
<u>MEAN QUANTITY</u>	<u>21/12Z</u>	<u>22/00Z</u>	<u>12 HR. CHANGE</u>
ω (MBAR/SEC $\times 10^{-3}$)	-1.5	-.9	+ .6
KINETIC (CAL/GRM)	.023	.023	0
UPPER HALF	.030	.039	+ .009
LOWER HALF	.015	.007	- .008
INTERNAL (CAL/GRM)	62.66	61.56	- .90
POTENTIAL (CAL/GRM)	14.13	15.33	1.20
LATENT HEAT (CAL/GRM)	2.00	1.96	- .04
ABS. VORT.	10.4	9.8	- .6
REL VORT. ($SEC^{-1} \times 10^{-5}$)	-.7	-.6	+ .1
UPPER HALF	-3.0	-2.3	- .7
LOWER HALF	1.5	1.1	- .4
FRONTAL INTENSITY $[-\frac{\partial \theta}{\partial Y}]$ (°C/111KM)	2.4	.9	-1.5
UPPER HALF	1.3	.3	-1.0
LOWER HALF	3.5	1.5	-2.0

Fig. 18. Schematic of Volume A (containing frontal zone) passing over Alps. Table lists mass weighted volume averages for 12Z 21 July 76 and 00Z 22 July 76 and time changes in: vertical motion; kinetic energy (in upper and lower half of volume), other energy quantities; absolute and relative vorticity (in upper and lower half); and frontal intensity (in upper and lower half).



<u>MEAN QUANTITY</u>	<u>21/12Z</u>	<u>22/00Z</u>	<u>12 HR. CHANGE</u>
ω (MBAR/SEC $\times 10^{-3}$)	+1.50	+ .54	- .96
KINETIC (CAL/GRM)	.019	.022	+ .003
UPPER HALF	.022	.033	+ .011
LOWER HALF	.015	.010	- .005
INTERNAL (CAL/GRM)	62.50	61.49	-1.01
POTENTIAL (CAL/GRM)	14.50	14.74	+ .24
LATENT HEAT (CAL/GRM)	1.80	1.72	- .08
ABS. VORT. ($\times 10^{-5} \text{ SEC}^{-1}$)	12.9	9.4	3.5
REL. VORT. ($\times 10^{-5} \text{ SEC}^{-1}$)	+1.5	- .5	-2.0
UPPER HALF	+2.0	0	-2.0
LOWER HALF	+1.0	- .9	-1.9
FRONTAL INTENSITY [$-\frac{\partial \theta}{\partial y}$] ($^{\circ}\text{C}/111\text{KM}$)	2.2	1.5	- .7
UPPER HALF	.5	1.0	+ .5
LOWER HALF	1.5	2.0	+ .5

Fig. 19. Schematic of Volume B (containing frontal zone passing over Pyrenees). Table lists mass weighted volume averages for 12Z 21 July 76 and 00Z 22 July 76 and time changes in: vertical motion; kinetic energy (in upper and lower half of volume), other energy quantities; absolute and relative vorticity (in upper and lower half); and frontal intensity (in upper and lower half).



<u>MEAN QUANTITY</u>	<u>21/22Z</u>	<u>22/00Z</u>	<u>12 HR. CHANGE</u>
ω (MBAR/SEC $\times 10^{-3}$)	+ .2	+1.7	+1.5
KINETIC (CAL/GRM)	.028	.024	- .004
UPPER HALF	.043	.039	- .004
LOWER HALF	.011	.010	- .001
INTERNAL (CAL/GRM)	61.88	61.78	- .10
POTENTIAL (CAL/GRM)	14.72	14.71	- .01
LATENT HEAT (CAL/GRM)	1.41	1.51	+1.0
ABS. VORT. (SEC $^{-1} \times 10^{-5}$)	13.7	12.0	-1.7
REL. VORT. (SEC $^{-1} \times 10^{-5}$)	3.0	3.0	0
UPPER HALF	4.5	4.0	-0.5
LOWER HALF	1.5	2.0	+ .5
FRONTAL INTENSITY [$-\frac{\partial \theta}{\partial Y}$] (°C/111KM)	2.0	3.2	+1.2
UPPER HALF	2.0	4.0	+2.0
LOWER HALF	2.0	2.5	+ .5

Fig. 20. Schematic of Volume C moving into Mediterranean. Table lists mass weighted volume averages for 12Z 21 July 76 and 00Z 22 July 76 and time changes in: vertical motion; kinetic energy (in upper and lower half of volume), other energy quantities; absolute and relative vorticity (in upper and lower half); and frontal intensity (in upper and lower half).

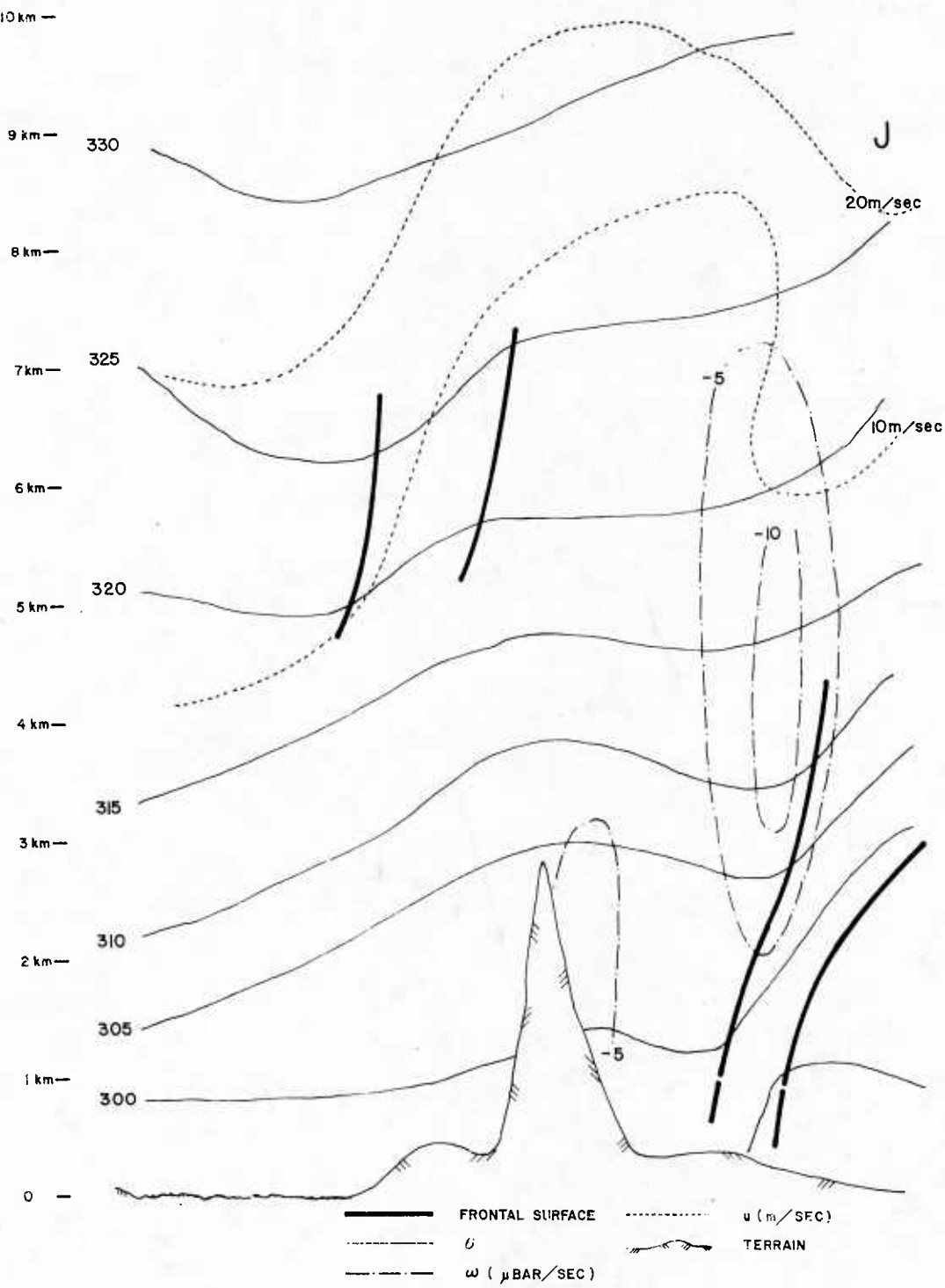


Fig. 21. Cross section through Volume A (along 11E) from 36° N to 55° N, illustrating frontal zone, potential temperature (θ), vertical motion (ω) and westerly wind component (u) for 12Z 21 July 76.

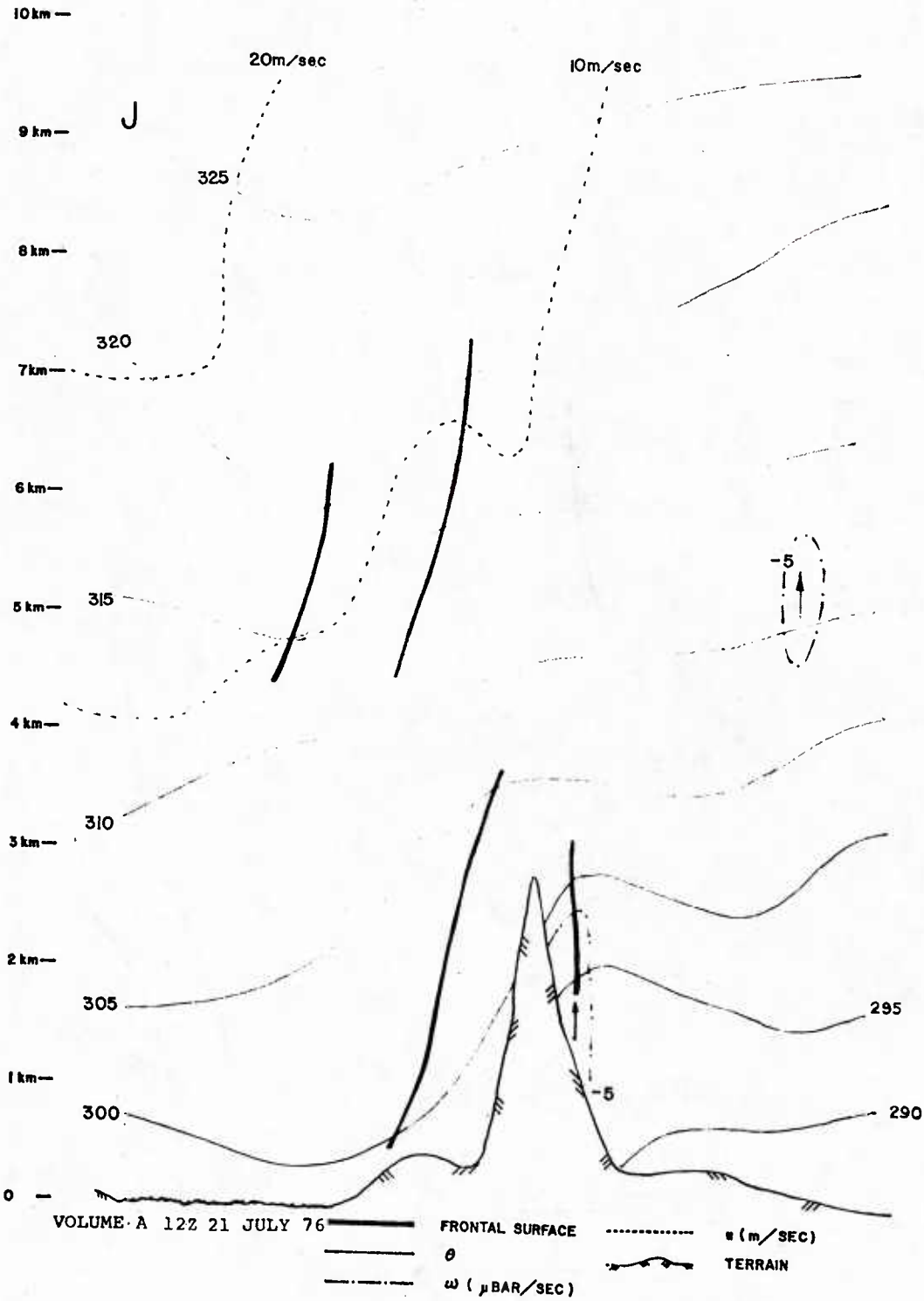


Fig. 22. Cross section through Volume A (along 11E) from 36° N to 55° N, illustrating frontal zone, potential temperature (θ), vertical motion (ω) and westerly wind component (u) for 00Z 22 July 76.

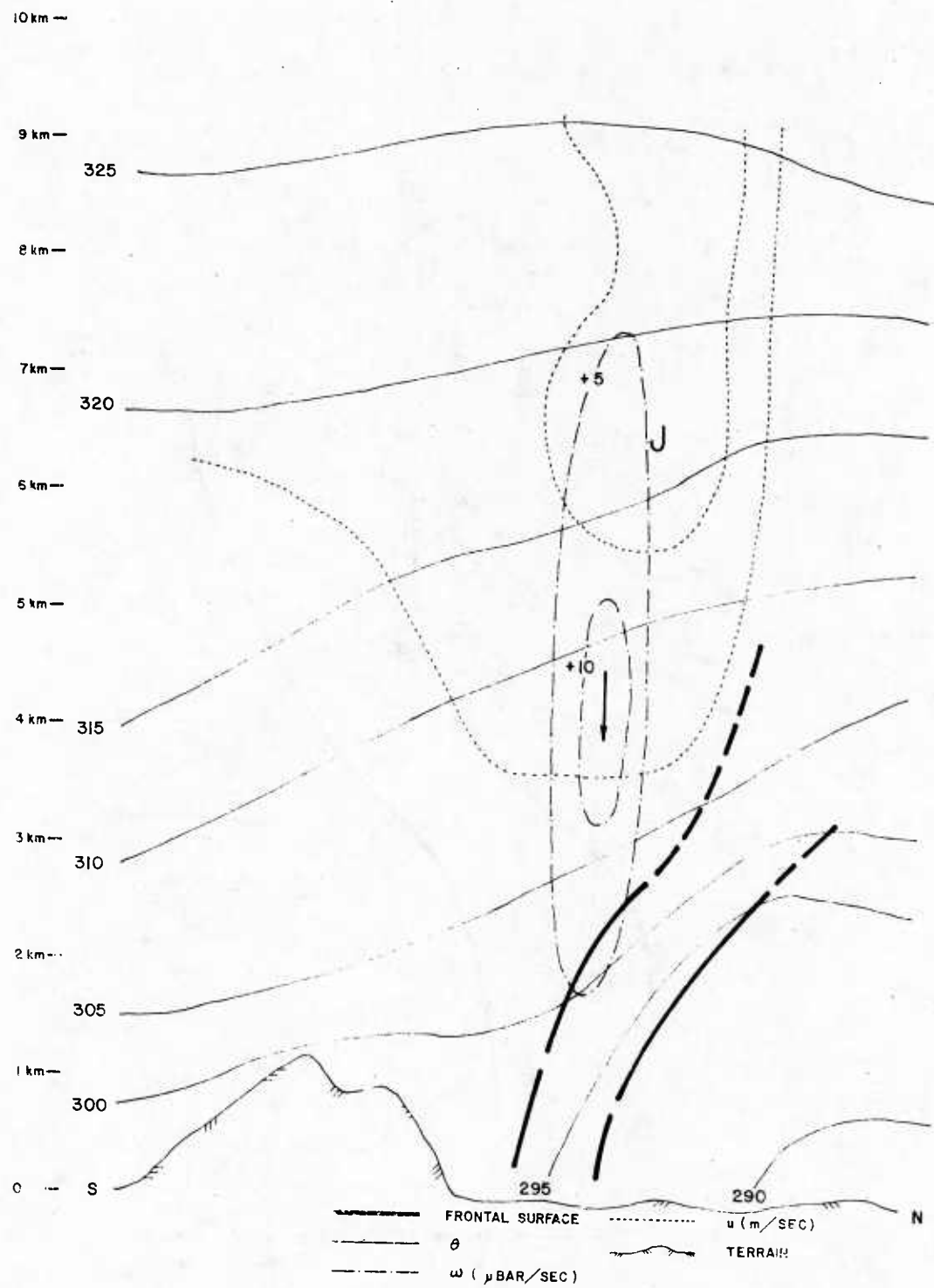


Fig. 23. Cross section through Volume B (along 1° W) from 36° N to 55° N illustrating frontal zone, potential temperature (θ), vertical motion (ω) and westerly wind component (u) for 12Z 21 July 76.

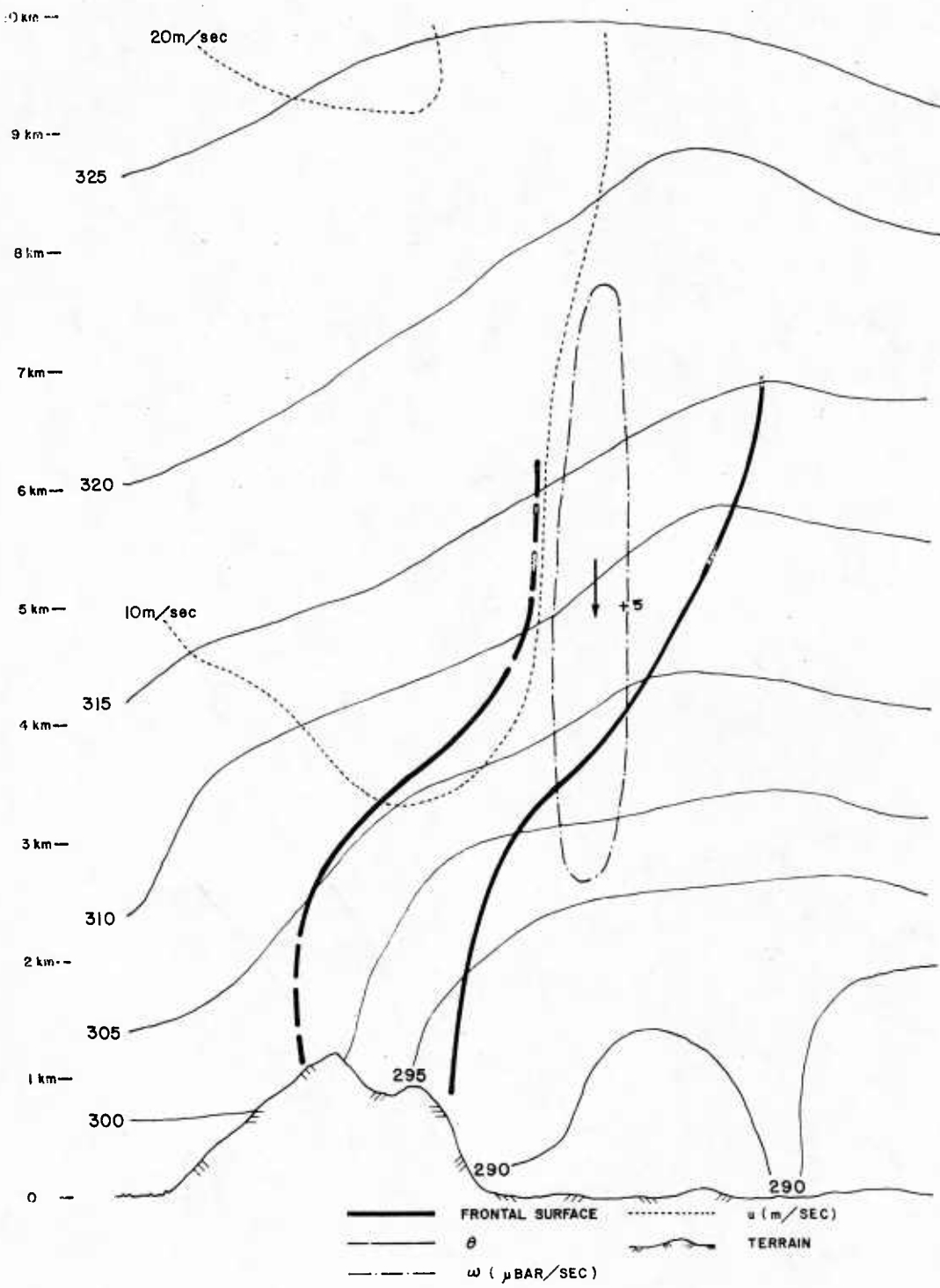


Fig. 24. Cross section through Volume B (along 1° W) from 36° N to 55° N illustrating frontal zone, potential temperature (θ), vertical motion (w) and westerly wind component (u) for 00Z 22 July 76.

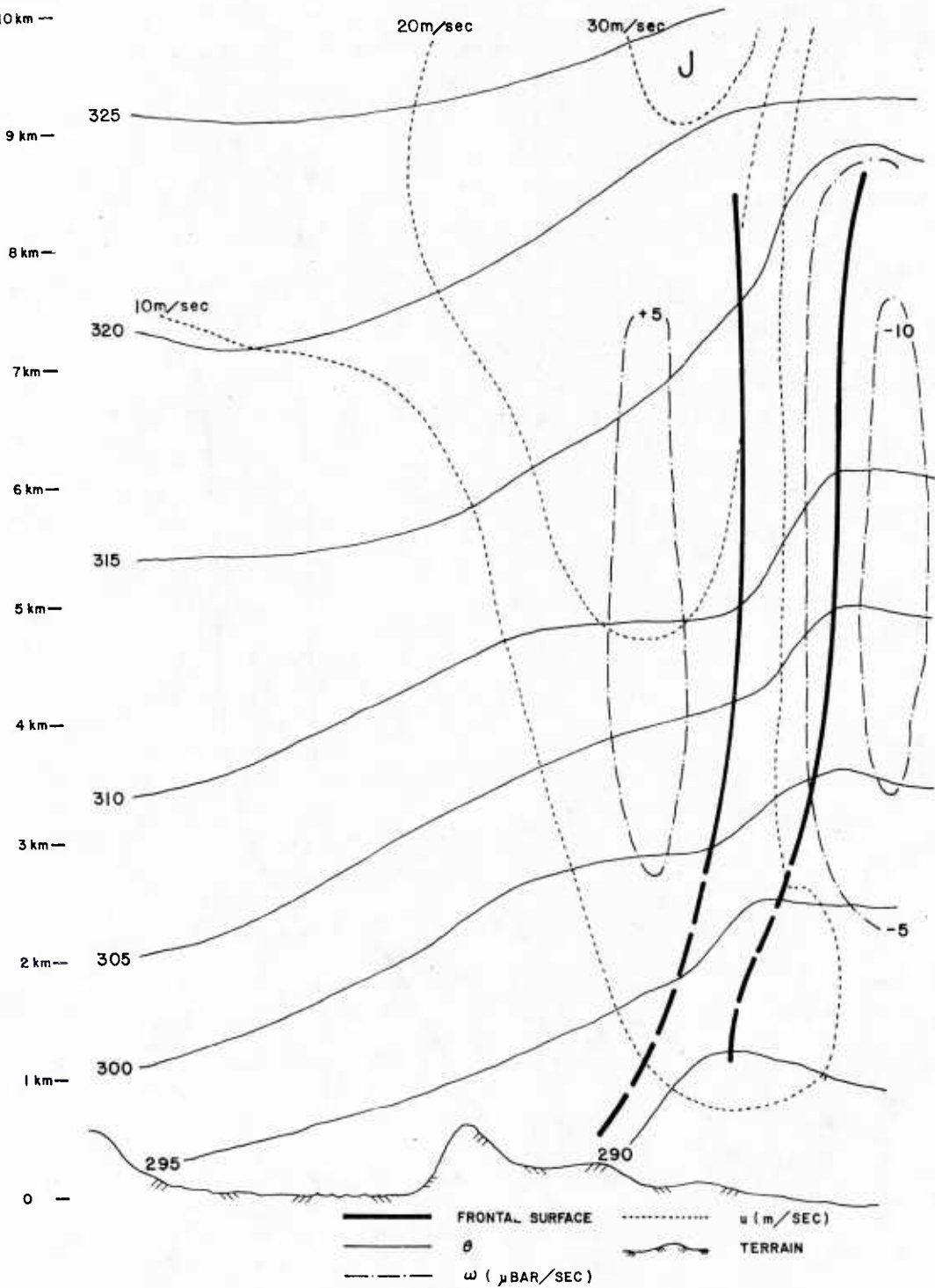


Fig. 25. Cross section through Volume C (along 5° E) from 36° N to 55° N illustrating frontal zone, potential temperature (θ), vertical motion (ω) and westerly wind component (u) for 12Z 21 July 76.

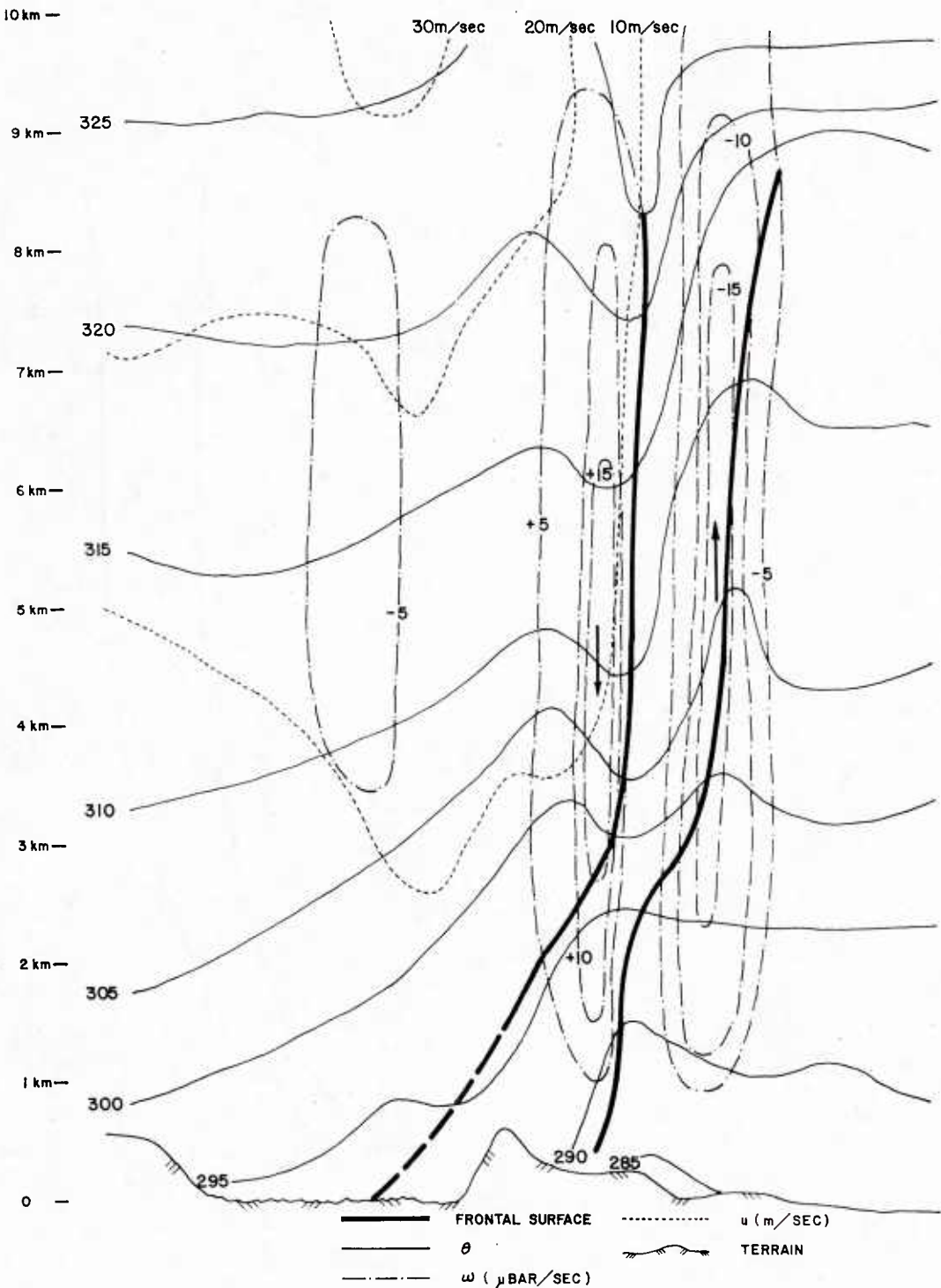


Fig. 26. Cross section through Volume C (along 5° E) from 36° N to 55° N illustrating frontal zone, potential temperature (θ), vertical motion (ω) and westerly wind component (u) for 00Z 22 July 76.

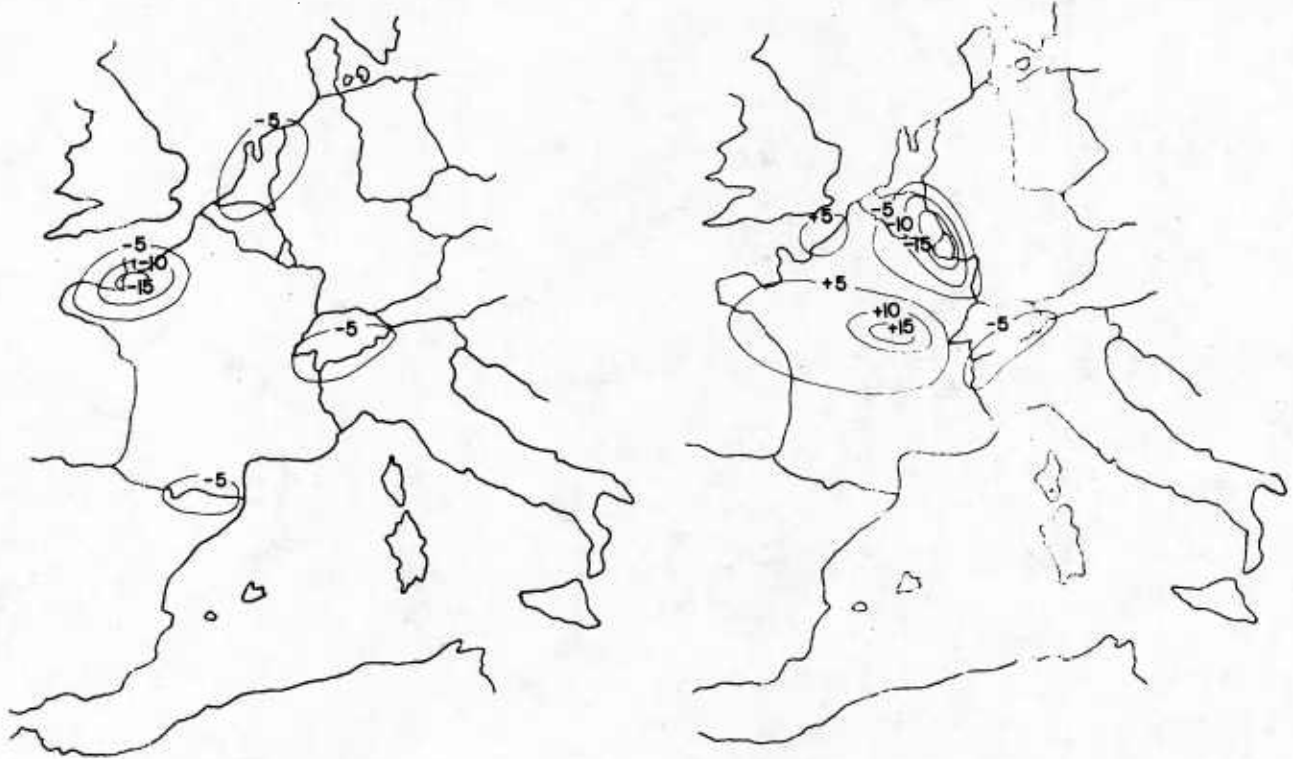


Fig. 27. Lagrangian kinetic energy tendency through whole atmospheric depth. For 21-22 July 76.

$$\left[\frac{d\left(\frac{1}{2} v^2 P_s \right)}{dt} \right] (\text{cal/m}^2 \text{ sec} \times 10^4)$$

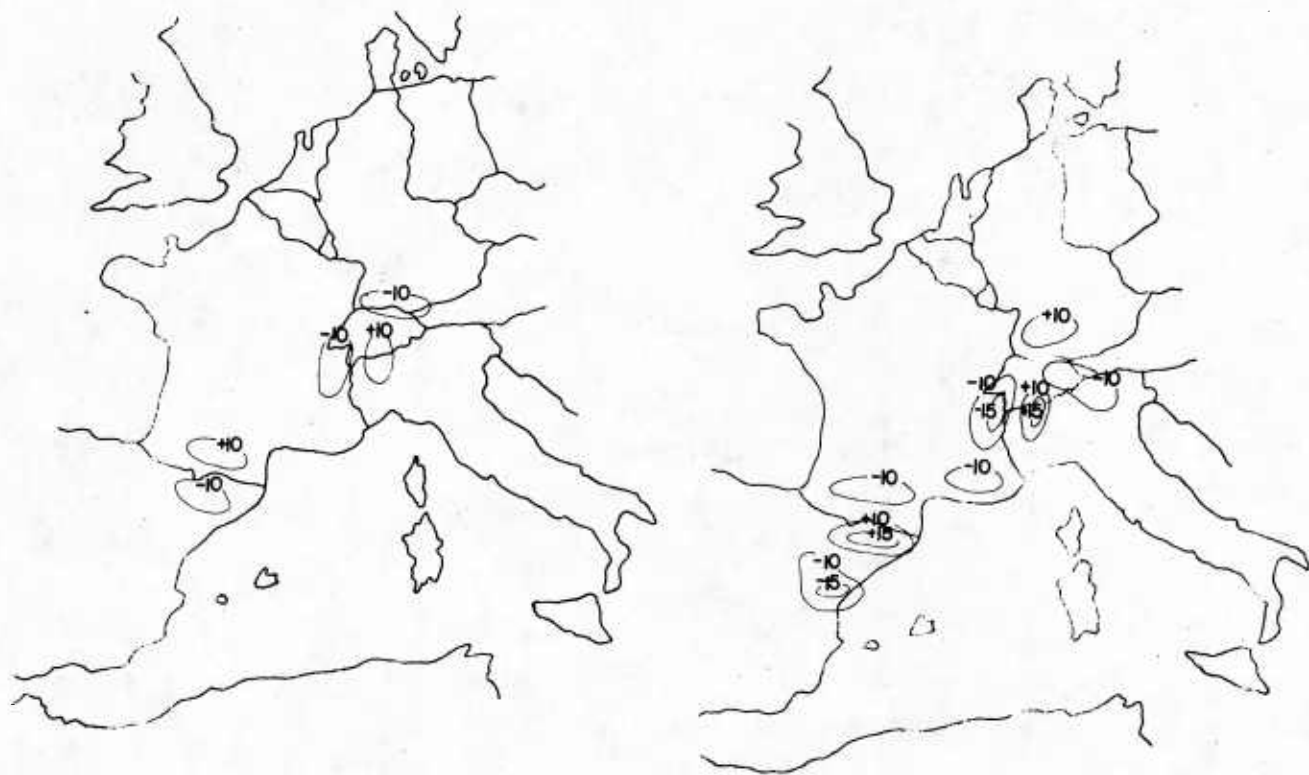


Fig. 28. Lagrangian enthalpy tendency through whole atmospheric depth for 21-22 July 76.

$$\left[\frac{d(C_p T_p)_s}{dt} \right] (\text{cal/m}^2 \text{ sec} \times 10^4)$$

- b) Energy budgets, while not balancing perfectly, contained only small errors which in most cases could be explained by energy source terms such as daytime heating or friction.
- c) Kinetic energy reduction in the lower half of each volume compares closely with the "roughness" or maximum height of the terrain encountered. See Figure 29.
- d) Not surprisingly, calculations of parcel tendencies indicate mountains act as KE sinks, and also as heat sinks on the windward side and heat sources in the lee. The latter phenomena tends to enhance the baroclinic zone or front as it passes over the mountain ridge. Figure 30 shows a schematic diagram of this mechanism.
- e) The net effect of moisture condensation in a frontal zone passing over terrain (higher than the lifted condensation level) is to slow, steepen and intensify the front. Figure 31 shows in a simple way how this is done. Comparison of the November (dry) case and the July (moist) case points this out. Fronts weakened less (even intensified) in low levels after the front passed the mountain barrier in the July case.

The moisture effect may also be seen in Case 2, volume A where the windshift line moved far in advance of the temperature gradient. The destabilization of air ahead of the front is a commonly seen feature in Pacific fronts, often producing strong gusty winds east of the Rockies in the dry air preceding the front.

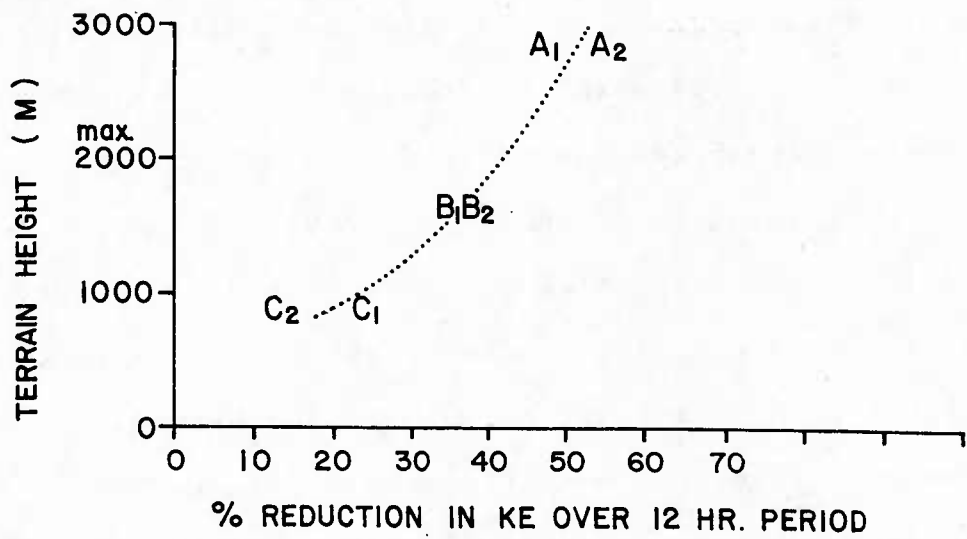


Fig. 29. Percent reduction (for 12 hours) in bulk kinetic energy in volumes A, B, C for Case 1 (Nov. 73) and Case 2 (Jul. 76) versus maximum terrain height along volume trajectory. (Plot A₁ indicates Volume A for Case 1).

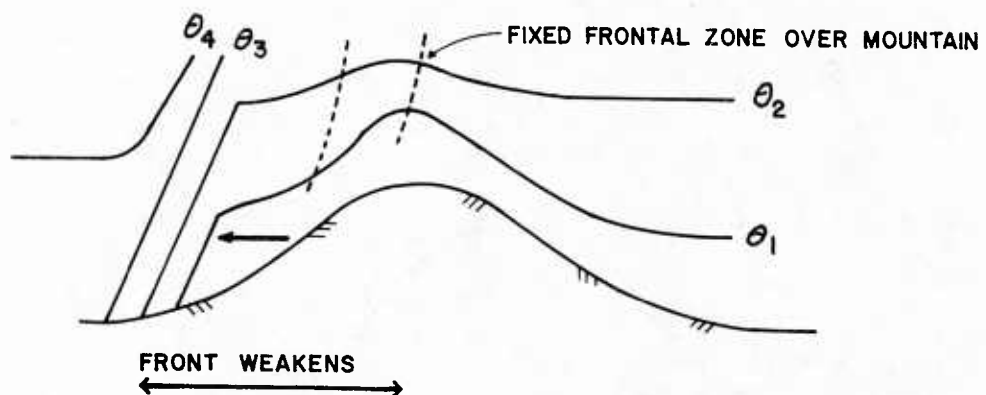
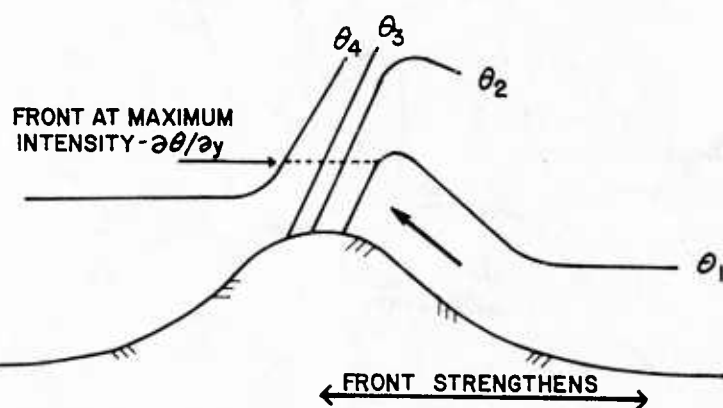
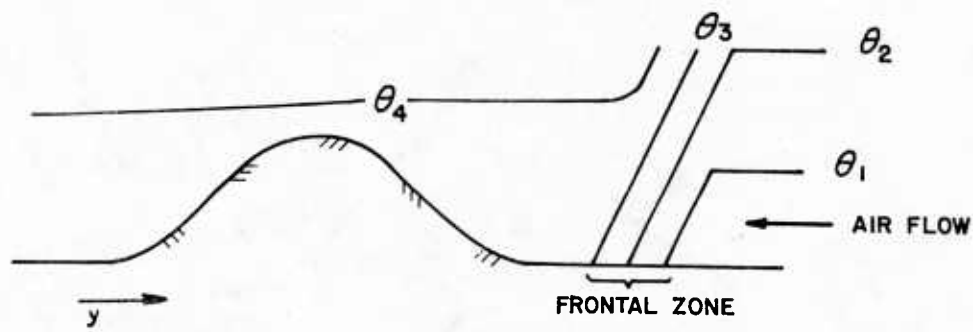


Fig. 30. Schematic diagram illustrating the effect of a mountain ridge on frontal intensity. Such an effect was seen in the case study analysis.

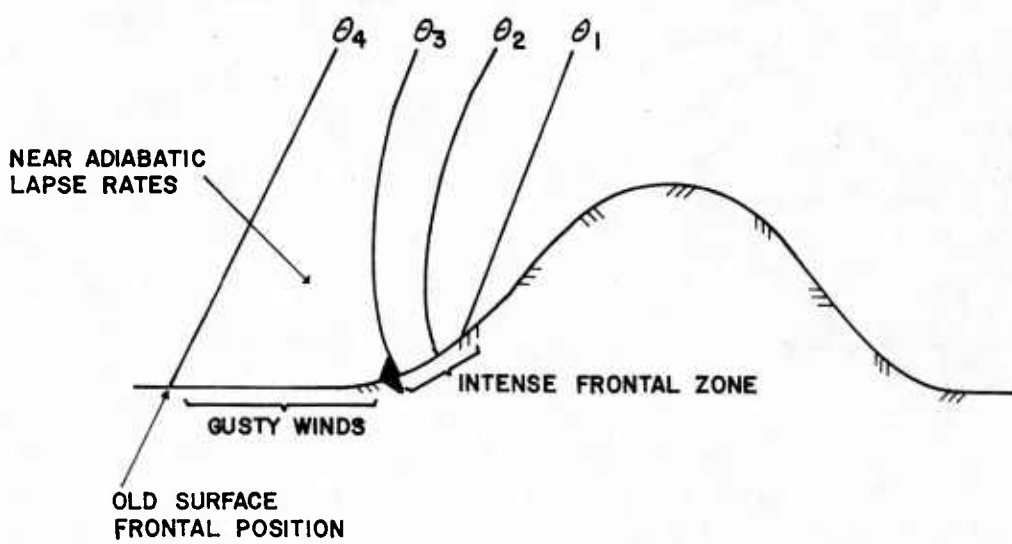
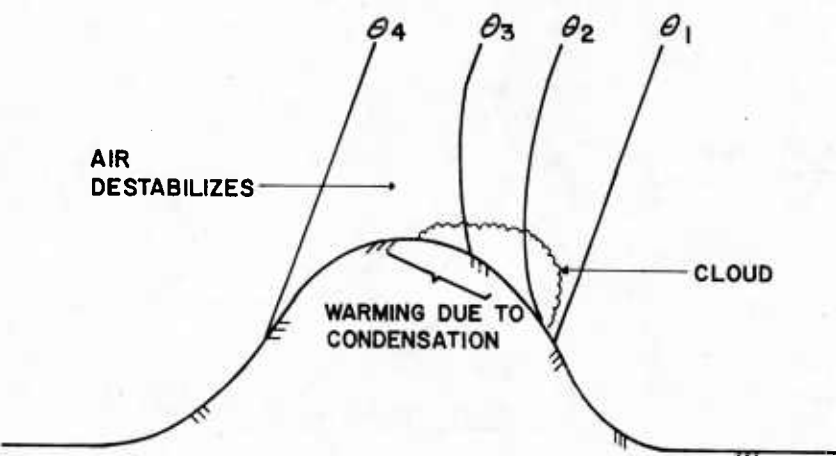
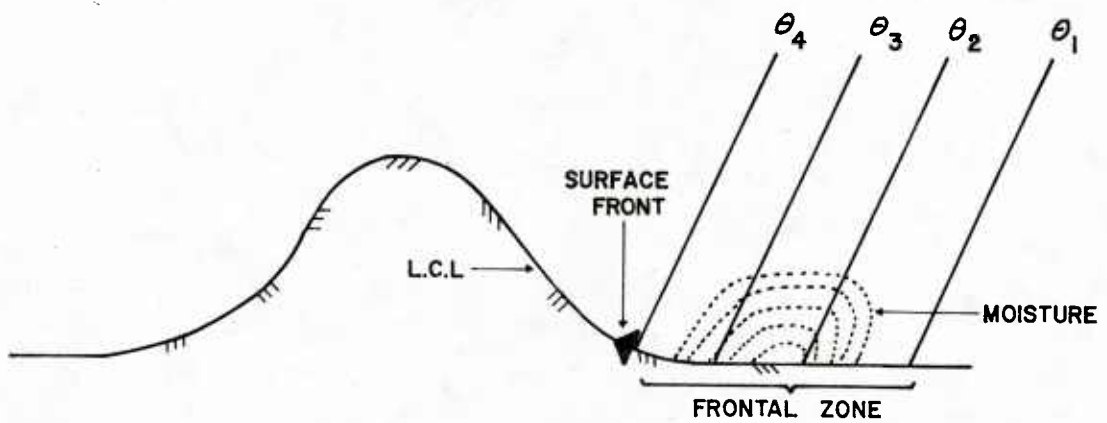


Fig. 31. Schematic diagram illustrating the effect of moisture on frontal intensity $[-\frac{\partial \theta}{\partial y}]$ passing a mountain ridge. The effect was seen $[-\frac{\partial \theta}{\partial y}]$ in the case study analysis.

- f) The use of vorticity equations as a diagnostic tool was not too successful. Increases in vorticity above the mountain crest observed in some cases were partially explained by the tilting term, but continuity with respect to potential vorticity was difficult to interpret. Loss of low level vorticity may be due to mountain frictional effects.
- g) Heat and kinetic energy flux data were gathered, but time limits prevented meaningful interpretation.

REFERENCES

- Berkovitz, L. D., 1961: Variational methods in problems of control and programming, J. Math. Anal. and Appl., 5, 145-169.
- Bleck, R., 1977, Numerical simulation of lee cyclogenesis in the Gulf of Canada, Mon. Wea. Rev., 105, p. 428-445.
- Buzzi, A., and S. Tribaldi, 1977, Inertial and frictional effects on rotating and stratified flow over topography, Quart. J. R. Met. Soc., 103, pp. 135-150.
- Haltiner, G. J., Numerical Weather Prediction, John Wiley and Sons, New York, 1971, 317 pp.
- McGinley, J., Environmental energy fields associated with severe storms, 1973, Masters Thesis, University of Oklahoma, 130 pp.
- Ninomiya, K., 1968, Heat and water budget over the Japan Sea and Islands in winter season, J. Meteor. Soc. Japan, 46, 343-372.
- _____, and S. Matsumoto, 1969, Objective analysis of the thermodynamic field consistent with the energy supply and cumulus distribution, J. Meteor. Soc. Japan, 47, 98-108.
- Palmer, E. and C.W. Newton, 1969: Atmospheric circulation systems. Academic Press; New York, London. 603 pp.
- Sasaki, Y., 1958: An objective analysis based on the variational method. J. Meteor. Soc. Japan, 36, 77-88.
- _____, 1969: Proposed inclusion of time variational terms, observational and theoretical, in numerical variational analysis. J. Meteor. Soc. Japan, 47, 115-124.
- _____, 1970: Some basis formalisms in numerical variational analysis. Mon. Wea. Rev., 98, 875-883.
- _____, Y. K., T. L. Baxter and J. L. McGinley, 1977, Final Report on Contract No. N0028-76-C-3160, 63 pp.
- Trevisan, A., 1977, Numerical experiments on the influence of orography on cyclone formation with an isentropic equation model, Jour. Am. Sci., 33, 768-780.
- Wagner, K. K., 1971: Variational analysis using observational and low pass filtering constraints. M.S. Thesis, University of Oklahoma, 39 pp.

APPENDIX A

USE OF VARIATIONAL INEQUALITY CONSTRAINTS IN ADJUSTMENT OF VERTICAL TEMPERATURE PROFILES

The goal of this work in objective analysis is to impose upper or lower limits on one or more meteorological quantities, this being combined with observational and dynamical constraints which have been well documented (Sasaki, 1958, 1969, 1970).

This class of constraint has been known and in use in engineering, particularly in control problems.

The strong inequality constraint can be reduced to a more familiar strong constraint problem or Bolza problem by the use of the Valentine-Berkovitz Theorem, which introduces an unknown function termed the "slack" function (Berkovitz, 1961).

To illustrate, consider the present problem. Temperature fields are objectively analyzed using low pass variational filters (Wagner, 1971). However, in the vertical, instrument problems or low data density occasionally produce spurious super adiabatic layers. For a variety of reasons it is desirable to remove these layers by re-adjusting the temperatures to conform to neutral stability constraints (which are consistent with the scale of our analysis).

Thus the condition on the temperature becomes:

$\frac{\partial \theta}{\partial \pi} \geq 0$ where θ is potential temperature and π is the vertical coordinate.

At this point we introduce the unknown slack function $D(\pi)$, which allows us to write the constraint as an equality:

$\frac{\partial \theta}{\partial \pi} = D^2(\pi)$ Note that $D^2(\pi)$ (if real valued) is positive for all π .

The variational formalism can now be expressed as:

$$J = \int_0^{\pi_0} [\alpha(\pi) (\tilde{\theta} - \theta)^2 + \lambda(\pi) (\frac{\partial \theta}{\partial \pi} - D^2(\pi))] d\pi$$

where α is an observational weight function (a function of π), $\tilde{\theta}$ is the "observed" or unadjusted temperature, $\lambda(\pi)$ is the Lagrange multiplier associated with the strong constraint stated above. θ , λ , and D and all unknown functions which must be determined.

Taking the variation and setting it equal to 0 allows us to find the functions λ , D , θ which minimize J .

$$\delta J = \int_0^{\pi_0} [2 (\tilde{\theta} - \theta) \delta \theta + (\frac{\partial \theta}{\partial \pi} - D^2) \delta \lambda + \lambda \frac{\partial \delta \theta}{\partial \pi} - 2\lambda D \delta D] d\pi = 0$$

After integrating by parts and collecting terms, and assuming the variations are arbitrary through the domain $[0, \pi_0]$, (we assume natural boundary conditions on λ [$\lambda_0 = \lambda_{\pi_0} = 0$]) the three Euler-Lagrange equations are obtained.

$$1) \quad 2\alpha (\theta - \tilde{\theta}) - \frac{\partial \lambda}{\partial \pi} = 0$$

$$2) \quad \frac{\partial \theta}{\partial \pi} - D^2 = 0$$

$$3) \quad \lambda D = 0$$

Combining, we get:

$$\frac{\partial^2 \lambda}{\partial \pi^2} - 2\alpha(D^2 - \frac{\partial \theta}{\partial \pi}) - 2 \frac{\partial \alpha}{\partial \pi} (\theta - \tilde{\theta}) = 0$$

This equation is put into finite difference form and solved by an iterative-relaxation. Throughout the computation the condition expressed by eqn. 3 is imposed.

Figure A1 shows unadjusted and adjusted θ profiles. The weight α can be set for each level depending on the quality of data. Figure A3 shows $\alpha(\pi_1)$ with a low weight (suspected instrument error: possible wet temperature element at π_1). Figure A2 shows $\alpha(\pi_1)$ with a weight equal to other levels for circumstances where the atmosphere (or analysis scheme) may be producing short lived super adiabatic layers.

It should also be noted that if $\alpha(\pi)$ is constant for all π then the condition $\lambda_0 = \lambda_{\pi_0} = 0$ forces conservation of the mean potential temperature within the layer.

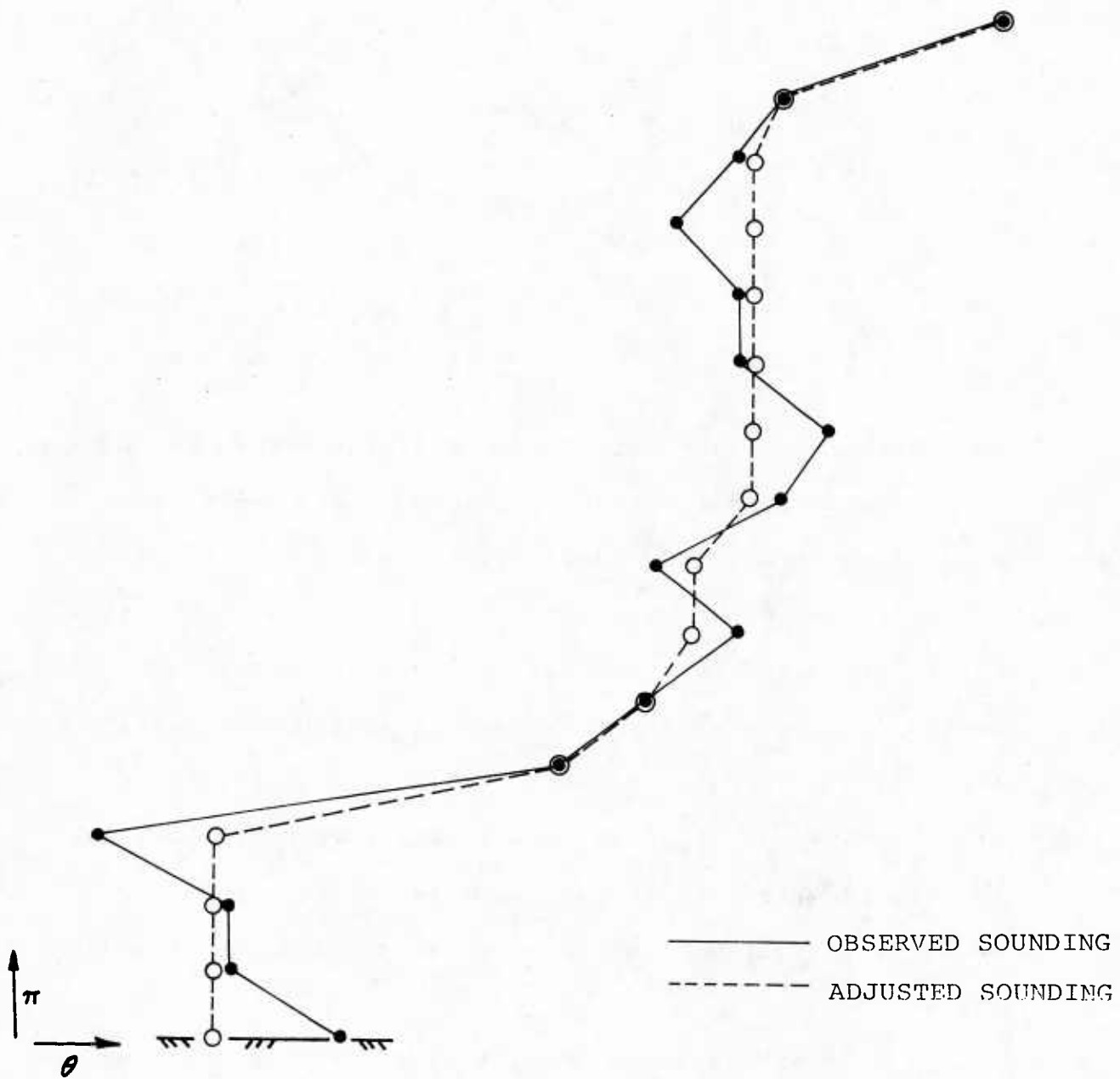


Fig. A1. Hypothetical "observed" and adjusted potential temperature profiles using inequality constraint.

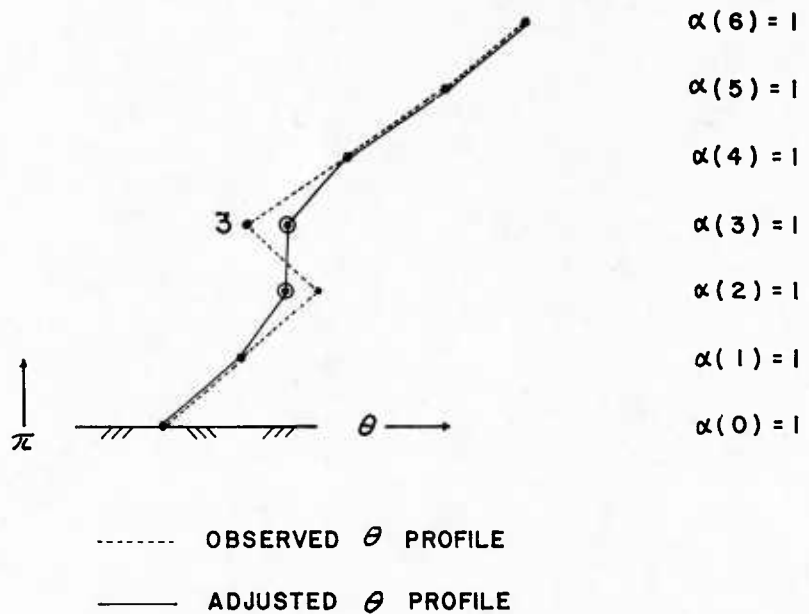


Fig. A2. Hypothetical "observed" and adjusted potential temperature profiles for equal weighting case ($\alpha(K)$ for $K = 1, 6$). Here data at 3 is assumed to be due to actual (though possibly short lived) atmospheric conditions.

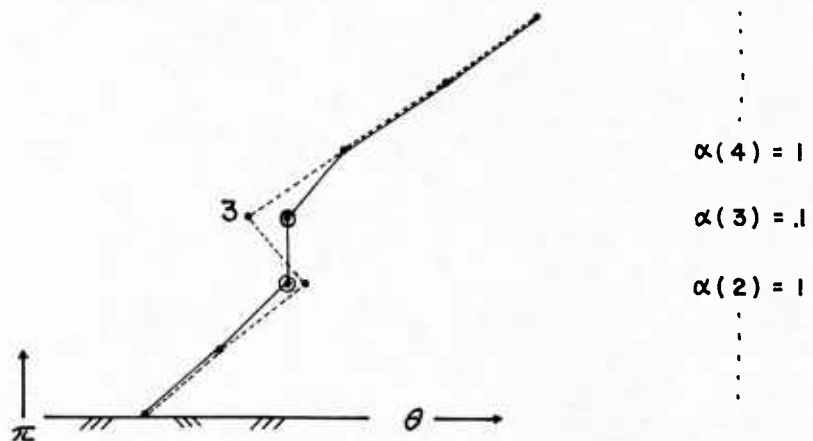


Fig. A3. Hypothetical "observed" and adjusted potential temperature profiles for non equal weighting ($\alpha(3) = .1$ $\alpha(K) = 1.0$) where error may be due to systematic instrument error such as rawinsonde exiting cloud layer.

DUDLEY KNOX LIBRARY - RESEARCH REPORTS



5 6853 01000469 0

U189375